frontiers in Materials

REVIEW
published: 18 January 2021
doi: 10.3389/fmats.2020.585602

Thermal–Mechanical Processing and Strengthen in $Al_xCoCrFeNi$ High-Entropy Alloys

Jinshan Li, Haoxue Yang, William Yi Wang, Hongchao Kou and Jun Wang**

State Key Laboratory of Solidification Processing, Northwestern Polytechnical University, Xi'an, China

In this study high-entropy alloys (HEAs) were devised based on a new alloy design concept, which breaks with traditional design methods for conventional alloys. As a novel alloy, HEAs have demonstrated excellent engineering properties and possible combinations of diverse properties for their unique tunable microstructures and properties. This review article explains the phase transition mechanism and mechanical properties of high-entropy alloys under the thermal-mechanical coupling effect, which is conducive to deepening the role of deformation combines annealing on the structure control and performance improvement of high-entropy alloys, giving HEAs a series of outstanding performance and engineering application prospect. To reach this goal we have explored the microstructural evolution, formation of secondary phases at high and/or intermediate temperatures and their effect on the mechanical properties of the well known $Al_xCoCrFeNi$ HEAs system, which not only has an important role in deepening the understanding of phase transition mechanism in $Al_xCoCrFeNi$ HEAs, but also has important engineering application value for promoting the application of high-entropy alloys.

Keywords: high-entropy alloy, thermal–mechanical processing, microstructure, strengthen, mechanical property

OPEN ACCESS

Edited by:
Lai-Chang Zhang, Edith Cowan University, Australia

Reviewed by:
Songqin Xia, University of Science and Technology Beijing, China
Yiping Lu, Dalian University of Technology, China

****Correspondence:***
Jinshan Li
ljsh@nwpu.edu.cn
Jun Wang
nwpuwj@nwpu.edu.cn

Specialty section:
This article was submitted to Structural Materials, a section of the journal Frontiers in Materials.

Received: *21 July 2020*
Accepted: *02 December 2020*
Published: *18 January 2021*

Citation:
Li J, Yang H, Wang WY, Kou H and Wang J (2021) Thermal–Mechanical Processing and Strengthen in $Al_xCoCrFeNi$ High-Entropy Alloys. Front. Mater. 7:585602. doi: 10.3389/fmats.2020.585602

INTRODUCTION

The design and development of structural materials that are suitable for extreme environments such as high temperatures, cryogenic environments, or situations that involve irradiation and corrosion, etc., are a high priority in the fields of materials science and technology. Modern technological developments in engineering, particularly in the nuclear, turbine, and aerospace industries, require new structural materials to provide higher performance than the currently available commercial alloys. Cantor et al. (2004) and Yeh et al. (2004) took the lead in adapting the traditional design methodology of alloys in 2004 and proposed the novel concept of alloy design, in which five or more elements are mixed in equiatomic or near equiatomic concentrations, such that the high configurational entropy ΔS^{conf}_{mixing} could promote single-phase-disordered solid solutions formation, e.g., fcc-centered cubic (fcc), body-centered cubic (bcc) or hexagonal close-packed (hcp) disordered phase (Troparevsky et al., 2015; Yuan et al., 2017; Tan et al., 2018a; Lu et al., 2018). High-entropy alloys (HEAs), also called multi-principal element alloys (Senkov et al., 2015) or complex concentrated alloys (Gorsse et al., 2017), have attracted attention on account of their superior performance in many aspects and broad application prospects (Li et al., 2016; Wang et al., 2017c; Guo et al., 2017; Tan et al., 2017; Wang et al., 2018a; Tan et al., 2018b; Gao et al., 2019; George et al., 2020). The appearance of HEAs has made alloy design central to phase diagrams, making it possible to obtain more potentially unique microstructures and properties.

In the field of HEAs, solute and solvent cannot be applied in the conventional alloy and the theoretical strengthening system needs to be verified. The optimization of the mechanical properties of high-entropy alloys is thus challenging. Recently, studies have focused on overcoming the strength-ductility trade off, by introducing high-density nano-twins in the grains (Lu, 2016; Schneider et al., 2020), as processing fine grains combined with nanoscale precipitates even distribution within the grains (Zhao et al., 2020b; Guillot et al., 2020; Yu et al., 2020), controlling the lattice misfit between intermetallic nanoparticles and matrix (Miracle, 2015; He et al., 2016a; Zhang et al., 2019) and producing materials with a heterogeneous structure (Sun et al., 2018; Wu et al., 2019; Du et al., 2020). The successful preparation of eutectic high-entropy alloy (EHEA) provided a new way to optimize the phase structure of HEAs by combining the ductile phase (e.g., fcc solid-solution phase) with the hard phase (e.g., bcc solid-solution phase or intermetallics) (Lu et al., 2014; Tan et al., 2019). This structure design could be realized through a simple and effective way of thermal-mechanical processing, offering a feasible strategy for a new generation of high-strength and high-toughness HEAs. Through cold rolling and annealing processing, the size, volume fraction, and distribution of the nano-sized particles ($L1_2$-Ni_3(Ti, Al), $L2_1$-(Ni, Co)$_2$TiAl, sigma (σ) or μ intermetallic phases) formed within the fcc phase matrix of HEAs could be controlled effectively, improving strain hardening ability by interacting with dislocations in plastic deformation (He et al., 2016b; Liu et al., 2016). An excellent balance between strength and ductility was obtained in the as-cast $AlCoCrFeNi_{2.1}$ EHEA (Lu et al., 2014). After extra heavily cold rolling and annealing, it showed significant improvement in tensile properties, with an ultimate tensile strength (UTS) of 1,200 MPa and elongation to failure (e_f) ~12% (Wani et al., 2016). Through cold rolling and subsequent annealing, different types of precipitates were formed within the matrix of the $FeCoNiCrTi_{0.2}$ HEA, improving strength and ductility at the same time (Tong et al., 2019). It is expected that the mechanical properties of HEAs could be successfully tailored using simple thermo-mechanical processing and further extended to bulk engineer materials for industrial application.

Earlier studies have tended to focus on single-phase HEAs with equal atomic ratio. However, phase stability is easily be impacted by alloying or moderate temperature annealing, which has a further effect on mechanical properties (Zhang et al., 2017; Macdonald et al., 2019). In addition, there are often some fatal disadvantages concomitantly, in that poor fluidity and castability may cause considerable chemical inhomogeneity in single-phase HEAs (Lu et al., 2014; Lu et al., 2017). It is hard to achieve excellent balanced tensile properties, e.g., the single fcc phase HEAs are usually soft while the single bcc phase HEAs are hard and brittle (Wang et al., 2012; Guo et al., 2013; Liu et al., 2019b). Thus, researchers have increasingly kept a watchful eye on not only the single-phase HEAs but also multiphase HEAs. By altering the composition of the alloying elements, the results of Stepanov et al. (2015) showed that the volume fraction of σ phase was related to the concentration of accumulated Cr and V elements. It was reported that the addition of Ni in $AlCoCrFeMo_{0.5}Ni_x$ alloys promoted the formation of the fcc phase, and the Ni element was also found to be an effective fcc structural stable element (Juan et al., 2013). Among them, $Al_xCoCrFeNi$ HEAs have been perceived as potentially important engineering materials as the inherent crystal structure can evolve from fcc into bcc with the variation of Al concentration (Chou et al., 2009; Wang et al., 2012; Garlapati et al., 2020). It has attracted a wide range of research interest due to its excellent physical and mechanical properties (e.g., creep behavior, dynamical mechanical property, impact toughness, magnetic properties, and resistivity–temperature behavior) (Kao et al., 2011; Ma et al., 2014; Cao et al., 2016; Cieslak et al., 2018; Xia et al., 2018; Wang et al., 2019a; Zhao et al., 2020a; Wang et al., 2020).

This review reports on recent advancements in thermal-mechanical processing and its effect on microstructural evolution and phase transformation in $Al_xCoCrFeNi$ HEAs. It also correlates insights into the mechanical properties and strengthening of HEAs, especially the evolution of hardness, plasticity, and strength under tension and compression at room temperature as well as at high temperatures with the phase structure, are also correlated.

DEVELOPMENT AND MECHANICAL PROPERTIES OF $AL_XCOCRFENI$ HEAS

Development of $Al_xCoCrFeNi$ HEAs

In the initial stage of the HEA research field, the HEA systems containing Cu were widely exploited due to the improvement of plasticity (Cantor et al., 2004; Chen et al., 2004; Yeh et al., 2004; Wu et al., 2006; Tung et al., 2007; Sriharitha et al., 2013). However, Cu tended to segregate at grain boundary for its high enthalpy of mixing with other elements. Meanwhile, the $Al_xCoCrCuFeNi$ HEA system has been carefully studied and the variation of Al content was found to bring significant changes in microstructure and mechanical properties of $Al_xCoCrCuFeNi$ (Tong et al., 2005a; Tong et al., 2005b; Wu et al., 2006; Tung et al., 2007). The compressive properties of AlCoCrFeNi alloy without Cu were investigated, showing a combination of excellent compressive strength (~2004 MPa) and plastic strain (~32.7%) (Wang et al., 2008). The Cu-free $Al_xCoCrFeNi$ HEA system has subsequently received increasing attention in the last decade.

Effects of Al Addition on Microstructure of $Al_xCoCrFeNi$ HEAs

The resultant phases in all the investigated as-cast $Al_xCoCrFeNi$ HEA system (x = 0–3) were: only solid-solution structures, mainly fcc, bcc or their mixture (Kao et al., 2009; Li et al., 2009; Ma et al., 2014; Wang et al., 2014; Zuo et al., 2014; Niu et al., 2016; Xia et al., 2016; Gangireddy et al., 2018a; Gangireddy et al., 2018b; Liu et al., 2018; Zhou et al., 2018; Annasamy et al., 2019; Li et al., 2019; He et al., 2020). Alloys with low Al contents (x = 0–0.3) exhibited the simple fcc structure, as x exceeded ~0.5, the bcc phase formed out of the fcc solid solution phase. Spinodal decomposition occurred later with an increase in Al content, leading to the formation of ordered (NiAl-type) and disordered bcc (A2) phases. Rao et al. (2016) also reported a fcc-bcc crystallographic orientation relationship between the

precipitation and fcc matrix: (1) $(1-10)_{bcc}//(200)_{fcc}$ and $[001]_{bcc}//[001]_{fcc}$; (2) $(1-11)_{B2}//(2-20)_{fcc}$ and $[011]_{B2}//[11\sqrt{2}]_{fcc}$.

The mechanism of bcc phase formation in $Al_xCoCrFeNi$ has received much attention. Kao et al. (2009) investigated the microstructural evolution of as-cast, -homogenized (1,100°C/24 h), and -deformed (1,100°C/24 h + 50% CR) $Al_xCoCrFeNi$ ($0 \le x \le 2$) high-entropy alloys. They reported that the structure of as-cast was sequentially single fcc ($x < 0.45$), duplex fcc–bcc ($0.45 \le x \le 0.88$), and single bcc ($x > 0.88$). While the x intervals for the existence of duplex phase in -homogenized and -deformed $Al_xCoCrFeNi$ alloys are $0.30 \le x \le 1.17$ and $0.30 \le x \le 0.875$, respectively, indicating the widening of the range of two-phase regions after homogenization treatment. The Al element was found to be a bcc stabilizer in $Al_xCoCrFeNi$ alloys. Jasiewicz et al. (2015) elucidated the phase stability of $Al_xCoCrFeNi$ ($x \le 3$) HEAs based on experimental data and computational results and found that the fcc phase was more stable when $x < 0.62$, and the range of fcc/bcc two-phase region was $0.5 \le x \le 1.0$. Ogura et al. (2017) also illustrated the effect of Al addition on phase transition in $Al_xCoCrFeNi$ alloys via first principles electronic structure calculations and an increase in Al content lowered the total energy difference between fcc and bcc.

Thermodynamic Appraisal of $Al_xCoCrFeNi$ HEAs

To accelerate the characterization of the composition-structure-property relationship of $Al_xCoCrFeNi$ HEAs, a calculation of phase diagrams (CALPHAD) approach was developed to predict the phase relationship in previous studies (Xia et al., 2016; Butler and Weaver, 2017; Rao et al., 2017; Gwalani et al., 2018; Shi et al., 2018; Komarasamy et al., 2019).

Xia et al. (2016) successfully predicted the phase diagram of the $Al_xCoCrFeNi$ ($x = 0$–2) alloy system through the CALPHAD approach using the PanHEA database. The experimental observations of $Al_xCoCrFeNi$ (x = 0.1, 0.75 and 1.5, respectively) were consistent with the predicted equilibrium phases diagrams. The fcc phase was stable over a wide temperature range of 645–1434 C for $Al_{0.1}CoCrFeNi$ alloy, whereas decomposition occurred at lower temperatures below 500 C. In addition, the predicted primary phase is the fcc phase and the B2 phase for the $Al_{0.75}CoCrFeNi$ alloy and $Al_{1.5}CoCrFeNi$ alloy, respectively. Komarasamy et al. (2019) chose the aging condition based on the pseudo-binary phase diagram using the PANDAT HEA database to develop the Ni_3Al ($L1_2$-type), B2 (Al–Ni based), and Al_3Ni particles to strengthen the $Al_{0.5}CoCrFeNi$ alloy. The existence of B2 precipitates was predicted for all heat treatment conditions except for 550°C, where $L1_2$ phases formed. The experimental phase relationship agreed well with the calculated result. To understand the phase stability and transformation pathway of $Al_{0.3}CoCrFeNi$ alloy under different thermal treatments, Gwalani et al. (2018) calculated the molar fraction of equilibrium phases as a function of the temperature for the alloy. Based on the calculated equilibrium phase data, the fcc-based $Al_{0.3}CoCrFeNi$ alloy was metastable at 620°C, and thus providing the possibility for the formation of new phases. All of these suggest that this way of calculating equilibrium phase diagrams provides useful guidance for the prediction of phases in the $Al_xCoCrFeNi$ HEAs.

Mechanical Properties of $Al_xCoCrFeNi$ HEAs

The Al content has a significant impact on the mechanical properties of the $Al_xCoCrFeNi$ HEA system. With the Al addition, the as-cast $Al_xCoCrFeNi$ alloys become much stronger, arising from the formation of bcc structures. The transition from fcc to bcc led to the hardness values varying from ~120 to ~570 Hv (Wang et al., 2012). The as-forged $Al_xCoCrFeNi$ alloys exhibited excellent mechanical properties at both room and cryogenic temperatures. The yield strength and tensile strength of the $Al_{0.1}CoCrFeNi$ alloy reached 412 and 1,042 MPa, while the yield strength and tensile strength of the $Al_{0.3}CoCrFeNi$ alloy were 515 and 1,010 MPa at 77 K, respectively. Different from conventional alloys, the plasticity of HEAs increased significantly with the decrease of temperature (Li and Zhang, 2016).

Optimizing the thermal-mechanical processing of the low-Al $Al_xCoCrFeNi$ alloys is a promising method of enhancing mechanical properties. Recent studies have indicated that the combined strength-ductility results from the complex interplay between multiple strengthening mechanisms, which are created by cold rolling and subsequent annealing (Gwalani et al., 2020). A strong Hall–Petch hardening effect with refining grains could be obtained in single-phase $Al_{0.3}CoCrFeNi$ alloy (Gwalani et al., 2017). Aging the alloy at 550–900°C led to the precipitation of nano-scaled B2 and/or σ intermetallic precipitates. Complex reinforcement effects resulting from fine fcc grains, intermetallic B2, and/or σ grains resulted in the unusually high strength of $Al_{0.3}CoCrFeNi$ HEA. Furthermore, the atomic distribution of Al-rich nano-clusters within the fcc phase brought about additional strength in the CR-550 condition (Gwalani et al., 2020). The significant changes in the phase structure and mechanical properties induced by the Al addition make this alloy system a desirable candidate material for structural materials with tunable strength.

THERMAL INDUCED PHASE TRANSITION AND ITS EFFECT ON $AL_XCOCRFENI$ HEAS

Thermal Induced Phase Transformation

Thermodynamic Ways of Annealing

The fcc-type CoCrFeNi HEA was generally considered to be thermally stable in the as-cast condition. However, after annealing at 750°C for 800 h, composition decomposition occurred and the minor addition of Al could further shorten the duration (He et al., 2017). The annealing temperature is one of the key factors that determine phase compositions. Prolonged annealing could also promote the second phase to precipitate from the matrix or along the grain boundary. Therefore, the investigation for the phase equilibria and phase stabilities of a series of $Al_xCoCrFeNi$ HEAs is significant, since they could influence the material design for applications at an intermediate temperature and expected component lifetime.

The room and high temperature XRD (from 573 to 1,373 K) patterns of the $Al_xCoCrFeNi$ ($x = 0$–1.8) alloys demonstrated that

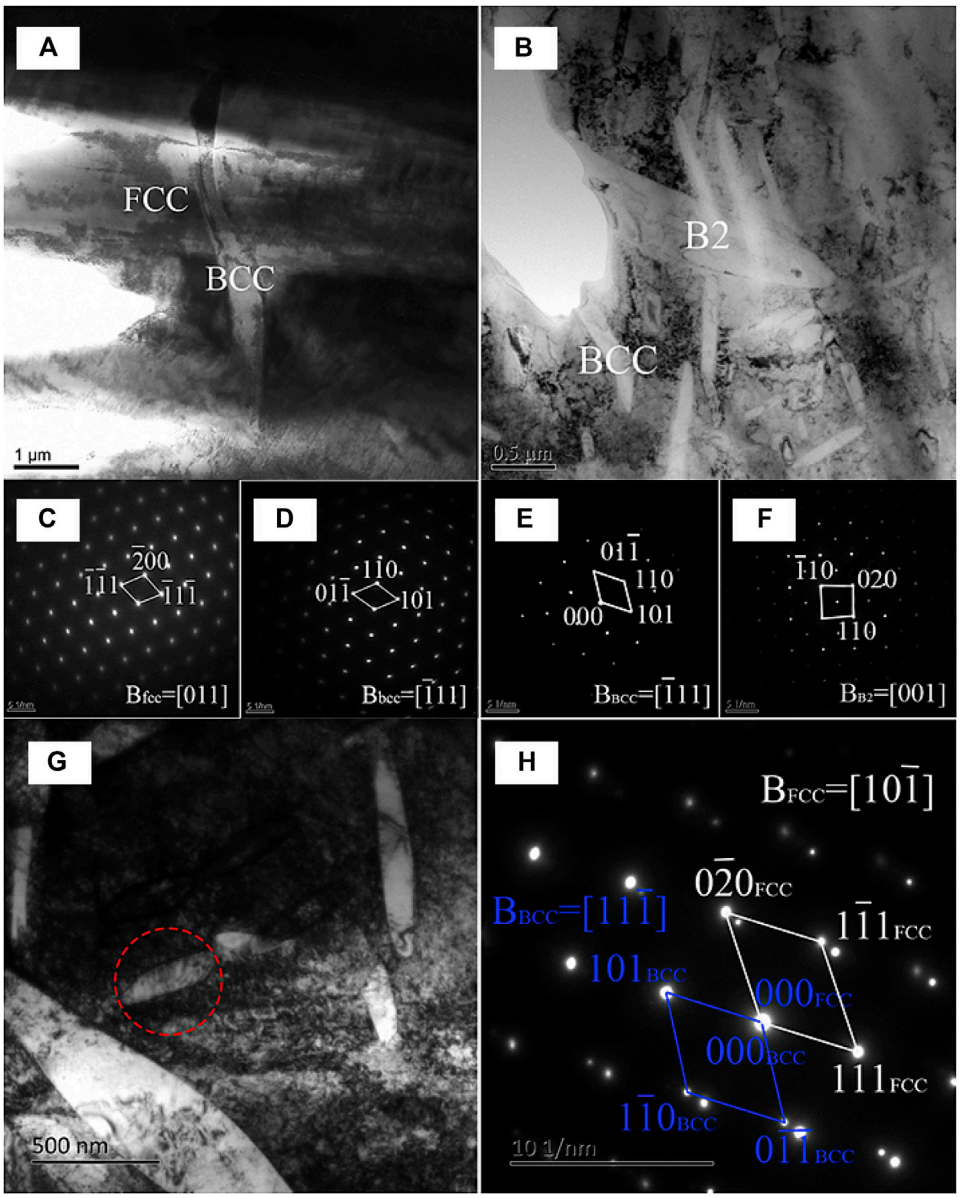

FIGURE 1 | TEM bright images **(A)** as-cast alloy, **(B,C)** corresponding selected electron diffraction imagem **(D,G)** heat-treated alloy at 1,123 K/8 h, and **(E–H)** corresponding selected electron diffraction image (Wang et al., 2017a). (Reprinted from Journal of Alloys and Compounds, Vol 710, Wang et al., The FCC to BCC phase transformation kinetics in an Al0.5CoCrFeNi high entropy alloy, Pages No.148, Copyright (2017), with permission from Elsevier).

crystal structure remained stable, except in $Al_{0.9}$–$Al_{1.2}$ alloys (Wang et al., 2014). The (Ni, Al)-rich acicular precipitates formed within the dendritic region of $Al_{0.5}$, while $Al_{0.3}$ remained a simple fcc phase with uniform composition after aged at 1,173 and 1,373 K for 2 h. A spinodal formed two-phase microstructure, consisting of disordered (Fe, Cr)-rich phase and ordered (Ni, Al)-rich phase, was observed in both as-cast $Al_{0.9}$ and $Al_{1.5}$ alloys. For the $Al_{0.9}$–$Al_{1.2}$ alloys, in line with the DSC analysis, the phase transition from bcc to fcc took place at 873 K and the appearance of σ phase was also observed at the temperature range of 873–1173 K, which depended on Al content. Butler and Weaver (2017) investigated the phase equilibria and phase stabilities of Al_xCoCrFeNi HEAs through methodically coupling the experimental results with predictions based on CALPHAD models. The coarsening of microstructures that consist of fcc, bcc, and/or ordered B2 phases occurred in all the alloys after annealing at 1,050°C. Annealing at 700°C conduced to stabilizing the mixed structure of fcc, bcc, B2, and/or σ phases depending on the relative concentration of Al. EDS analysis showed the Al depletion and Cr enrichment in fcc and bcc phases, respectively, while the B2 phase was enriched in Al and Ni, and the σ phase was enriched in Fe and Cr, respectively. The phase prediction by modeling coincided with the experimental results in $Al_{10}Co_{22.5}Cr_{22.5}Fe_{22.5}Ni_{22.5}$

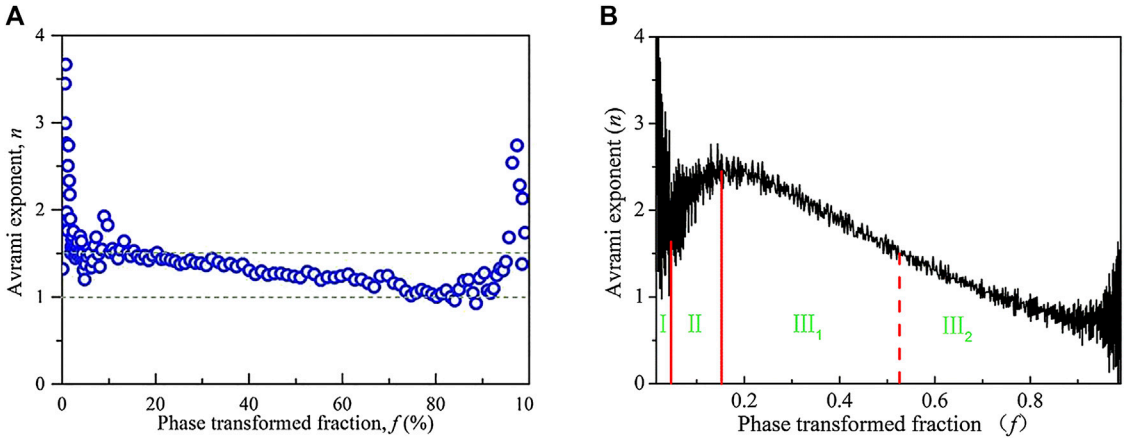

FIGURE 2 | (A) The local Avrami exponent (blue circle) as a function of phase transformed fraction of $Al_{0.25}CoCrFeNi$ HEA (4 K/min). The green zone represents the range of *n* from 1 to 1.5 (Wang et al., 2018b). **(B)** Variation in *n* with the increasing volume fraction of $Al_{0.5}CoCrFeNi$ HEA (3 K/min). (Wang et al., 2017a).

and $Al_{30}Co_{17.5}Cr_{17.5}Fe_{17.5}Ni_{17.5}$ HEAs but failed in $Al_{15}Co_{21.25}Cr_{21.25}Fe_{21.25}Ni_{21.25}$ and $Al_{20}Co_{20}Cr_{20}Fe_{20}Ni_{20}$ HEAs. The discrepancies were mainly related to destabilized components of the fcc phase at 700and 1,000°C. This indicated that CALPHAD based models were useful for predicting the phases formed in HEAs with complex components, but that the current thermodynamic database needs to be improved.

Nartu et al. (2020) investigated the effect of heat treatment on the microstructural evolution and mechanical properties of laser additively manufactured $Al_{0.3}CrFeCoNi$ HEA. The formation of the nano-scaled (Al, Ni)-rich clusters resulted from *in-situ* heat treatment during the part building and could act as the heterogeneous nucleation sites for the precipitates that form at high temperature aging. Nanometer-sized $L1_2$ or γ' type precipitation with spherical or rod-like morphology was predominantly revealed in the grain interior after being aged at 620°C for 50 h. Larger precipitates were also found at the grain boundaries of this condition and confirmed to be Al-rich B2 and Cr-rich σ phases. Niu et al. (2017a) investigated the influence of heat treatment on the microstructure of a fcc + bcc dual-phase $Al_{0.5}CoCrFeNi$ alloy. The alloy changed from dendritic into spherocrystal after being heat-treated at 650°C while rod-shaped phases and elliptoid phases rich in Al–Ni were precipitated after heat treatment at 1,150°C. The Al–Ni rich nano-sized B2 phase was also found to precipitate from the interdendritic (bcc) region after heat treatment at 650°C (Niu et al., 2016). Grain coarsening occurred after heat treatment at 850°C, and the fine bcc phase emerged and distributed uniformly in the matrix, as seen in **Figure 1** (Wang et al., 2017a). Another study reported the precipitation of a plate-like hexagonal closed-packed phase with high cobalt content located at the interdendritic region of the $Al_{0.5}CoCrFeNi$ HEA after 650°C/8 h heat-treatment (Wang et al., 2017b). Though a simple shear, the bcc phase could transform into the hcp phase, and the crystal orientation relationship between these two phases has also been to been established as $[11\text{–}20]_{hcp} \parallel [111]_{bcc}\ (000\text{–}1)_{hcp} \parallel (10\text{–}1)_{bcc}$. Liu et al. (2014) investigated the phase completion and stability of the AlCoCrFeNi alloy. They observed the phase transition from bcc and B2 to bcc and fcc after heat treatment at 950°C, indicating that the solid-solution phases of the as-cast alloy were unstable due to quenched-in chemical segregation. These studies suggest that the phase stability of $Al_xCoCrFeNi$ HEA should be carefully evaluated, especially at the intermediate temperature.

Kinetic Way of Tailoring Phases

The kinetic way is also important to the mechanism of phase evolution for HEAs. It is a way of establishing the reasonable heat treatment parameters to enhance performance. Wang et al. have inspected the phase transformation kinetics of the fcc $Al_{0.25}CoCrFeNi$ (Wang et al., 2018b) and fcc + bcc $Al_{0.5}CoCrFeNi$ (Wang et al., 2017a) HEAs during an experiment on isochronal heating by thermal dilation. The estimated activation energy and kinetic exponent were almost stable, indicating a slow and steady phase transition in an $Al_{0.25}CoCrFeNi$ HEA (**Figure 2A**). The phase transition was also a growth-controlled process without nucleation during the main transformation process, according to the decreasing trend from 1.5 to one of the determined kinetic exponent. The ordering transition from fcc to $L1_2$ occurred during the heat treatment at 650°C.

Compared with $Al_{0.25}CoCrFeNi$ HEA, three stages of phase transformation were characterized in $Al_{0.5}CoCrFeNi$ during the continuous heating process, and the third one corresponded to the fcc-bcc phase transition. Careful research into the microstructural evolution indicated that the first two stages of phase transformation involved nanoparticle precipitation (Niu et al., 2016; Niu et al., 2017a), whereas the transition from fcc to bcc took place in the third phase transformation. The three stages of the third phase transition were divided according to the determined Avrami exponent *n* (**Figure 2B**). Note that the third stage was divided into two parts, III_1 and III_2. The decrease of *n* indicated a reduced nucleation rate in III_1. In III_2

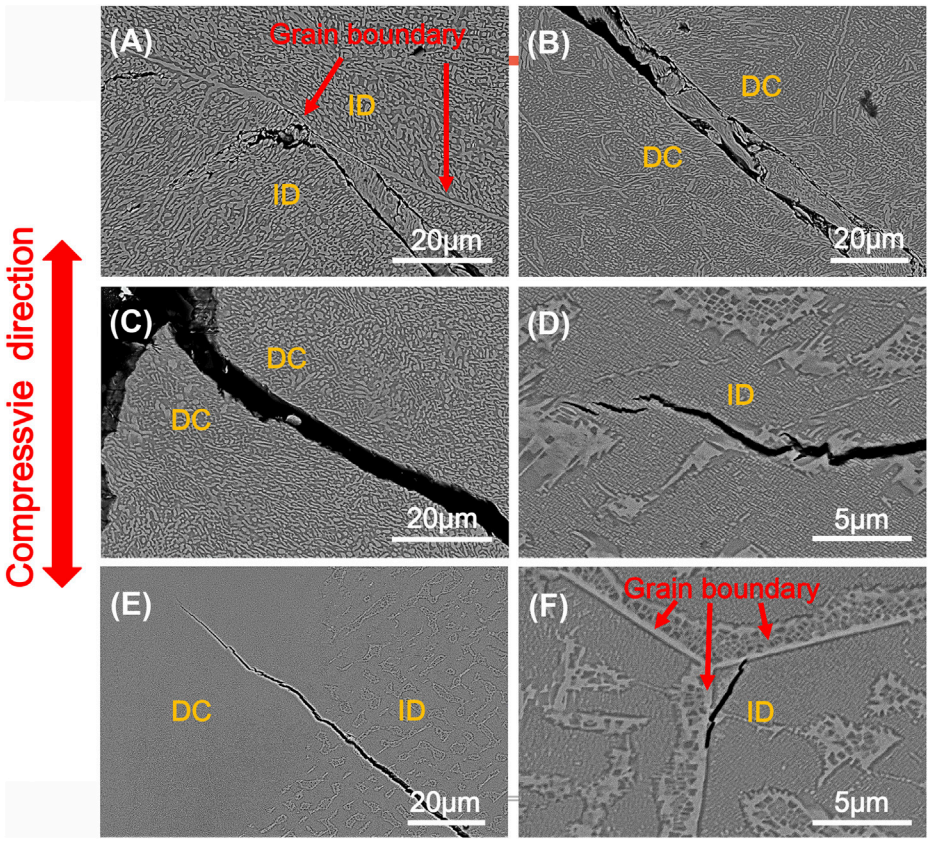

FIGURE 3 | Back-scattered election images of cracks after fracture in the compressive test at different processing temperatures **(A–C)** 950°C, **(D–F)** 1,200°C (Zhao et al., 2020a). (Reprinted from Journal of Alloys and Compounds, Vol 820, Zhao et al., Effect of strong magnetic field on the microstructure and mechanical-magnetic properties of AlCoCrFeNi high-entropy alloy, Pages No.5, Copyright (2020), with permission from Elsevier).

the formation of bcc structure led to a decrease of the concentration of bcc forming elements at the interface, thus further lowering the nucleation rate. The activation energy for $Al_{0.25}$CoCrFeNi (198 ± 1 KJ/mol) and $Al_{0.5}$CoCrFeNi (144–284 KJ/mol) HEAs was quite different, mainly due to the phase transition type differences between the two alloys, for the former it was order-disorder transition while the latter was an fcc-bcc transition. The kinetics of phase transformation in HEAs requires further exploration in future studies. In particular, it would be helpful to understand more about the phase selection through kinetic phase transformation and how this relates to annealing.

Mechanical Properties and Precipitation-Strengthening in Al_xCoCrFeNi HEAs

Niu et al. (2016) reported that annealing at 650°C for 0.5 to 8 h of $Al_{0.5}$CoCrFeNi HEA had a significant hardening effect, exhibiting the yield strength (YS) varying between 355 and 834 MPa strongly depending on the annealing time. The excellent tensile properties of alloy heat-treated for 8 h showed a YS of ~834 MPa with an elongation of 25%, which could be ascribed to the dispersed nano-sized B2 phase (~70 nm). After heat treatment at 850°C, the nano-sized B2 phase with a structure of thick slat and bcc phase with a structure of thin slat was formed in the fcc matrix. After heat treatment, a good combination of strength and plasticity was obtained by increasing the ultimate tensile strength up to 1,143 MPa and an elongation of 21.5% (Wang et al., 2017a). In $Al_{0.3}$CoCrFeNi HEA single crystals, only coherent particles of the γ'-phase were detected during aging 50 h at 893 K. The interaction of slip dislocations with γ'-phase particles occurred via a shearing mechanism and the contribution to the hardening from γ'-phase particles was 25–30 MPa. The absence of grain boundaries also suppressed the formation of B2-phase particles in $Al_{0.3}$CoCrFeNi HEA single crystals (Kireeva et al., 2020).

In another example for AlCoCrFeNi HEA, heat treatment at 850°C caused the phase transformation of the bcc matrix to the σ phase, drastically increasing the micro-hardness of the interdendritic region. The brittle σ phase then transformed back to the bcc matrix when heat-treated at 975°C, causing the alloy to soften, with lower micro-hardness but larger elongation. Homogenization treatment was conducted at a temperature above 1,200°C, leading to an increase both in compressive strength and compressive contraction (Munitz

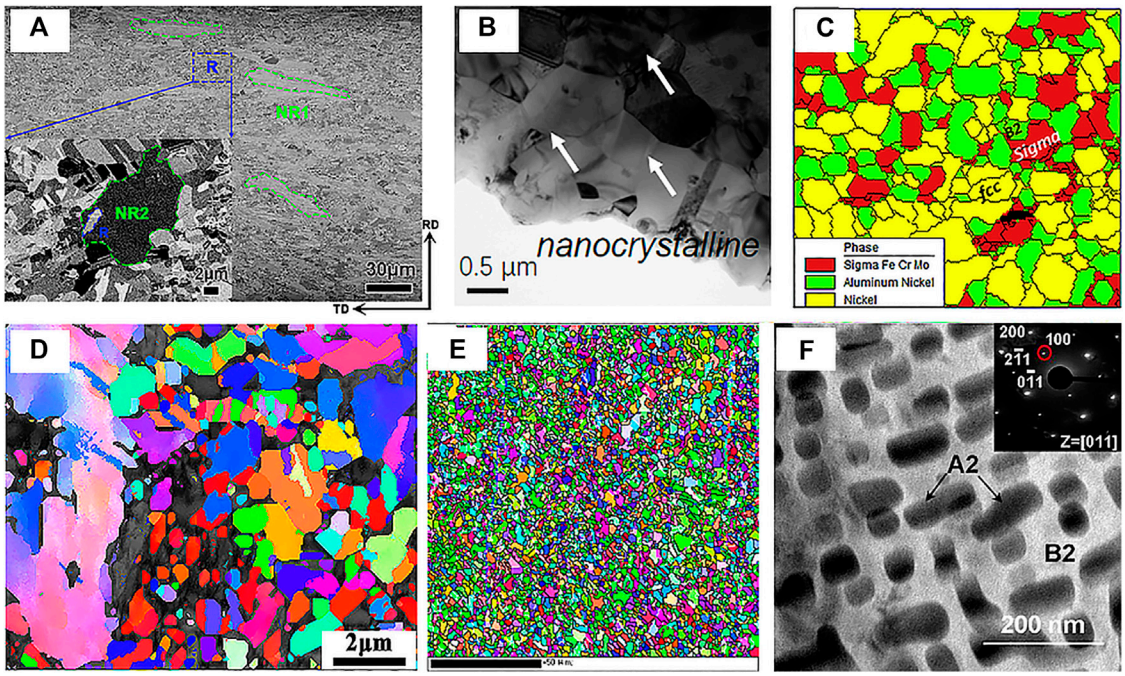

FIGURE 4 | Example microstructures of $Al_xCoCrFeNi$ HEAs under different conditions **(A)** BSE image of the 873 K-annealed $Al_{0.1}CoCrFeNi$ HEA, showing the microstructure composed of three types of grains: stretched original grains, partially recrystallized grains of large size, and completely recrystallized grains of fine size (Wu et al., 2019). **(B)** Nanocrystalline $Al_{0.25}CoCrFeNi$ HEA generated by directly annealing after cold rolling (He et al., 2020). **(C)** Tri-phase $Al_{0.3}CoCrFeNi$ HEA consisting of fcc, B2 and σ phases (Gwalani et al., 2018). **(D)** Ultrafine-grained $Al_{0.45}CoCrFeNi$ HEA generated in the recrystallization area after annealing at 800°C (Hou et al., 2019). **(E)** Fully-recrystallized $Al_{0.5}CoCrFeNi$ HEA with refined grains (Guo et al., 2018). **(F)** Cuboidal participates with the side length ranging from 20 to 180 nm, randomly distributed in the B2 matrix of $Al_{0.7}CoCrFeNi$ HEA (Shi et al., 2018).

et al., 2016). Zhao et al. (2020a) reported that with increasing temperature from 950to 1,200°C, the increased bcc phase and disappeared σ phase could improve the compressive properties of AlCoCrFeNi with both the YS and strain increased from ~1,069 to 1,254 MPa and ~17–~21%, respectively. Phase distribution was found to strongly influence the initiation and propagation of the cracks. They observed that cracks could propagate and terminate in both the dendrite (**Figures 3B,C,E**) and interdendritic region (**Figures 3A,D,F**) of the two samples. Besides, cracks changed the propagation route and then terminated at grain boundaries in the interdendritic region, which consisted of bcc matrix and B2 precipitates (**Figures 3A,F**), rather than stopping at the fcc grain boundaries.

THERMO-MECHANICAL COUPLING EFFECT

Microstructure Evolution After Thermo-Mechanical Treatment

Since the effect of heat treatment on mechanical properties was limited, numerous methods including rolling, forging, tension, compression and torsion, were then adopted to strengthen the materials by inducing the plasticity of the HEAs (Yu et al., 2016; Hou et al., 2017a; Guo et al., 2018). Optimized thermal-mechanical processing by deformation and subsequent annealing could lead to the grain refinement and formation of the strengthening phase. **Figure 4** exhibits the microstructures of ultrafine grains and/or nanostructured precipitates generated simply through cold deformation and annealing under different conditions (Guo et al., 2018; Gwalani et al., 2018; Shi et al., 2018; Hou et al., 2019; Wu et al., 2019; He et al., 2020). In the meantime, Wang et al. (2018c) investigated the effect of cold rolling on the fcc to bcc transformation kinetics of the $Al_{0.5}CoCrFeNi$ HEA and concluded that pre-deformation induced defects could facilitate the nucleation and growth process during the phase transition compared with the as-cast sample.

Effect of Cold Deformation and Annealing on the Microstructure

In general, thermo-mechanical processing is usually used to break and refine the coarse as-cast grains and/or second phases. However, the increase in strength was almost always along accompanied by decreased work hardenability due to the reduced dislocation storage capability of the refined structure. Therefore, a rational design of the thermo-mechanical processing is needed, to improve both strength and ductility. This section describes the effect of cold deformation and subsequent annealing on the microstructure of $Al_xCoCrFeNi$ HEAs. It reviews the recrystallization and grain growth of $Al_xCoCrFeNi$ alloys, and

the effect of aging at an intermediate temperature phase structures is presented afterward.

Yang et al. (2019c) reported the gradient effect on grain size in cold-rolled and annealed $Al_{0.1}CoCrFeNi$ alloys. The yield strength and grain size followed the classical Hall–Petch relationship, exhibiting a grain boundary hardening efficient of 464 MPa $\mu m^{1/2}$. Wu et al. (2019) have proposed a promising way to enhance the comprehensive mechanical properties of bulk high-entropy alloys by simple cold rolling and subsequent annealing at an intermediate temperature of 873 K. A heterogeneous structure with three types of grains was successfully generated including deformed grains, partially recrystallized grains (volume fraction of ~37%), and fully recrystallized-equiaxed grains, with a volume fraction of ~10, 37, and 53%, respectively, as shown in **Figure 4A**. The phase remained in a single fcc phase after the cold-rolled $Al_{0.25}CoCrFeNi$ was annealed at 1,100°C for 10 h (Hou et al., 2017b). The grain size was reduced from 230 to ~13 μm through multiple cold rolling and annealing processes (He et al., 2020), as shown in **Figure 4B**. The grain size could also be adjusted in a wide range in a single fcc phase $Al_{0.3}CoCrFeNi$ alloy (Gwalani et al., 2017). The fcc-based $Al_{0.3}CoCrFeNi$ HEA was dramatically transformed to a duplex fcc- ordered B2 (Choudhuri et al., 2018b) and even a tri-phase consisting of fcc, B2, and σ phases (**Figure 4C**) by tuning the cold rolling and annealing at a temperature of 800°C and 620°C, respectively (Gwalani et al., 2018). The strength enhancement due to grain boundary strengthening obeyed the Hall-Petch relationship and the Hall–Petch coefficient in $Al_{0.25}$ and $Al_{0.3}$ alloy was ~784 and 824 MPa $\mu m^{1/2}$, respectively. The high Hall–Petch coefficient observed in the $Al_xCoCrFeNi$ (x = 0.1–0.3) alloy indicated that dislocation motion is more difficult in $Al_xCoCrFeNi$ (x = 0.1–0.3) HEA than conventional alloys.

Hou et al. (2019) investigated the grain growth behavior of cold-rolled $Al_{0.45}CoCrFeNi$ alloy after heat treatment at 700–1,100°C. Shear bands could still be retained after annealing at 800°C due to recrystallization. Ultrafine recrystallized fcc grains with an average grain size of 0.62 μm were generated, as shown in **Figure 4D**. The grain-growth exponent (n) is estimated to be 3.4, which was attributed to the fact that the grain corner-distributed B2 precipitation effectively hindered grain growth. The microstructure of the cold-rolling (**Figure 4E**) and subsequent annealing of $Al_{0.5}CoCrFeNi$ HEA has also been investigated (Guo et al., 2018; Yang et al., 2019a). The reported recrystallization temperature (~0.81 T_m; T_m referring to the melting point) in the alloy was attributed to coarse as-cast grains, severe lattice distortion effect, and sluggish diffusion effect. The dispersed bcc particles at grain boundaries could effectively slow the grain growth when annealing at 1,200°C with a holding time extended to 16 h.

After cold rolling, a large number of crystal defects such as dislocations are produced in the material, which store high deformation energy. Through subsequent annealing, the stored energy could be released and the deformed structure recrystallizes to refine the grains. The ideal structures could be obtained via reasonable heat treatment, i.e., ultrafine-grain structure, or heterogeneous structure. Meanwhile, high-entropy alloys exhibited a rather high recrystallization temperature and strong resistance to grain growth during annealing, mainly due to the precipitates in the vicinity of the grain boundaries effectively suppressing the grain coarsening of the fcc matrix.

Effect of Hot Deformation and Annealing on the Microstructure

The investigation of hot deformation and dynamic recrystallization mechanisms in $Al_xCoCrFeNi$ alloys is vital, considering the current interest in employing HEAs for critical high temperature applications. Haghdadi et al. (2020b) investigated the hot-worked microstructure of an $Al_{0.3}CoCrFeNi$ alloy. Most deformation bands were poorly developed even at high strains due to the intrinsic resistance of the lattice to dislocation movement in HEA. The alloy softened through dynamic recrystallization, mainly occurring at the initial grain boundaries through the grain boundary migration caused by strain then followed by multiple twinning chains and the formation of micro-shear bands. Hot deformation at 1,030°C under the strain rate of 0.1 s^{-1} was mainly conducted through the matrix phase in $Al_{0.6}CoCrFeNi$ and $Al_{0.9}CoCrFeNi$ alloys (Haghdadi et al., 2020a). Discontinuous dynamic recrystallization (DDRX) occurred at the interphase boundary mantle regions in the fcc matrix of $Al_{0.6}CoCrFeNi$ alloy, along with local subgrain coalescence. With further deformation, the DDRX regions expanded and covered most of the microstructure at a strain of 1.5. While in the $Al_{0.9}CoCrFeNi$ alloy, the bcc matrix mainly underwent continuous dynamic recrystallization. No evidence of DDRX in the BCC phase of $Al_{0.9}CoCrFeNi$ was observed even at the highest strain level of 1.5.

Rao et al. (2017) investigated the formation of the second phase in the forged $Al_xCoCrFeNi$ (x = 0.3, 0.5, 0.7) alloys via an *in-situ* TEM heating study. The forged alloys mainly consisted of fcc and B2 phases (Ni, Al)-rich $L1_2$ nanoprecipitates were observed in the fcc matrix of forged $Al_{0.5}CoCrFeNi$, while the Cr-rich bcc phase existed within the B2 phase. Many twins also formed within the fcc phase in all the as-forged alloys due to the low stacking fault energy (Kumar et al., 2015; Choudhuri et al., 2019), whereas high local deformation was present in the B2 region. Two types of precipitates were observed using an *in-situ* TEM study, a Cr-rich σ phase, and an Al-rich θ phase (an $Al_{45}Cr_7$ type). They also described the σ phase precipitation in detail using a thermodynamic calculation. One observation was that the σ phase could nucleate at the bcc/B2 interface, where the Cr-rich bcc phase forming in the B2 region would then decompose. The other observation was that the σ phase directly from the fcc matrix. The homogenization effect of 1,250°C heat treatment on the forged $Al_{0.7}CoCrFeNi$ HEA was investigated by Shi et al. (2018). A net-like A2 (disordered) phase and nano-sized spherical A2 particles were distributed in the B2 matrix in the as-forged $Al_{0.7}CoCrFeNi$ alloy. After being heat-treated at 1,250°C for 1,000 h, the as-equilibrated $Al_{0.7}CoCrFeN$ showed a morphological transformation of the A2 phase, changing from being net-like nano-particles to cuboidal participates that were randomly distributed in the B2 matrix, as shown in **Figure 4F**.

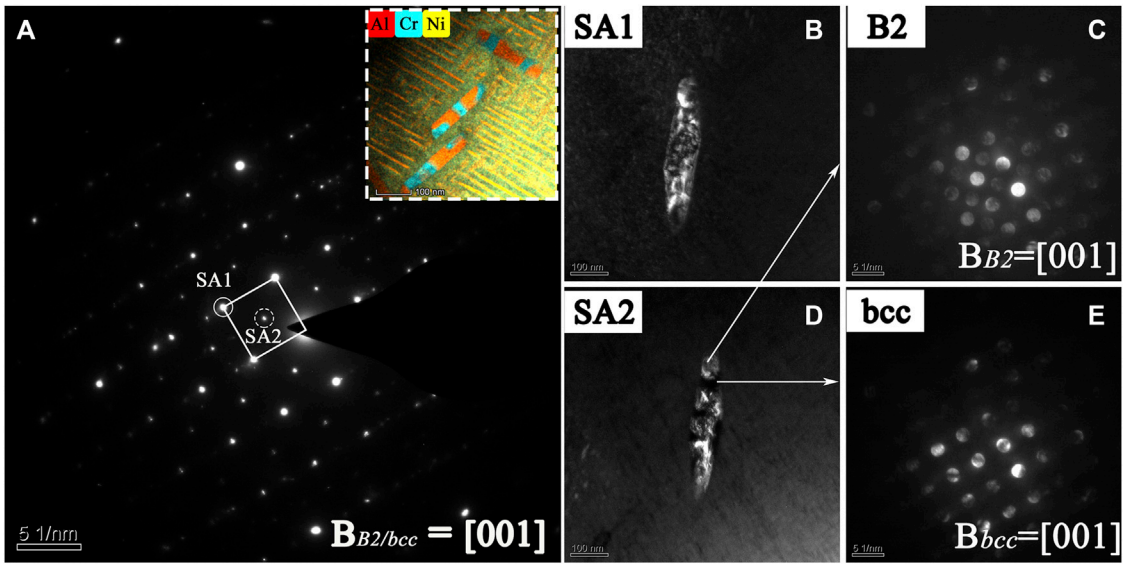

FIGURE 5 | (A) the SADP image from the [001] $_{bcc}$ zone axis of the B2/bcc region with the image of HAADF-EDS **(B,D)** dark field images from the [001]$_{B2/bcc}$ zone axis, and **(C,E)** the corresponding electron diffraction patterns of the CRSA-140 $Al_{0.5}$CoCrFeNi alloy (Yang et al., 2020). (Reprinted from Journal of Materials Science & Technology, Vol 72, Yang et al., Nanophase precipitation and strengthening in a dual-phase Al0.5CoCrFeNi high-entropy alloy, Pages No.6, Copyright (2021), with permission from Elsevier).

Research on the hot deformation of Al_xCoCrFeNi high-entropy alloys is still rare. The softening mechanism within the fcc and/or bcc phases could be influenced by the varying of Al concentration. Meanwhile, the heat treatment after hot deformation at homogenization temperature was certified to have a profound influence on simplifying the microstructure and reducing the elemental segregation. Research exploring the hot deformation behavior of high entropy alloy is at a preliminary stage and further studies on the microstructure evolution and property improvement of the alloy after deformation are needed.

Precipitation at Intermediate Temperatures

Recent studies indicate that Al_xCoCrFeNi HEAs display a significant age-hardening phenomenon. Precipitation at intermediate temperatures of the famous fcc-based $Al_{0.3}$CoCrFeNi alloy has been reported by many researchers. An aging treatment that was used to fully-recrystallize $Al_{0.3}$CoCrFeNi HEA at 550°C for 150 h and 700°C for 50 h, resulted in the formation of ordered $L1_2$ Ni_3(Ti,Al)-type precipitates dispersed in the interior of the grains and B2 precipitates forming along the grain boundaries, respectively (Gwalani et al., 2017). The lath-like B2 precipitates exhibited an orientation relationship with the fcc matrix. The stable nano-scale B2 precipitates were also found along the twin boundary in close proximity to the fcc matrix (Wang et al., 2019b). A combination of both nano-scaled ordered $L1_2$ precipitates and grain boundary B2 precipitates were obtained after being aged at 620°C for 50 h (Gwalani et al., 2017).

Concurrent recrystallization and precipitation occurred after being directly aged at 550°C for 24 h and 620°C for 50 h of 90% cold-rolled $Al_{0.3}$CoCrFeNi alloy and microstructures consisting of tri-phase (fcc + B2 + σ) were obtained. A dual-phase (fcc + B2) structure was produced after being aged at 900°C for 0.5 h, and only the fcc phase was detected after being aged at 1,100°C (Gwalani et al., 2020). The grain size had a significant impact on the annealing-induced phase transformation in $Al_{0.3}$CrFeCoNi HEA. In the coarse-grained alloy, the fcc phase transformed to the ordered $L1_2$ phase and finally to the B2 phase with increasing temperature, while the No $L1_2$ phase formed during the annealing process of the nanocrystalline alloy (Tang et al., 2016). The grain boundaries in the nanocrystalline HEA could provide a channel for the rapid diffusion of elements to form the high-temperature stable B2 phase at a relatively low temperature, thereby inhibiting the formation of the $L1_2$ ordering.

The fcc phase remained disordered after being heat treated at 1,100 °C in cold-rolled $Al_{0.7}$CoCrFeNi HEA, while the B2 to B2+bcc transformation occurred in the B2 lamellae. Subsequent low temperature annealing treatment at 580 °C for 24 h introduced nano-scaled order $L1_2$ precipitates in the fcc lamellae. B2/bcc phases were also found in the fcc + $L1_2$ region (Gwalani et al., 2019). The formation of similar conjoint B2/bcc phase during the process of annealing was also reported in $Al_{0.5}$CoCrFeNi alloy, as shown in **Figure 5** (Yang et al., 2020). The compositional differences are visible within the Al-Ni rich B2 regions (**Figure 5A**), suggesting the presence of Cr rich nano-precipitates, resulting from the coherent interfaces between the two phases and driven by the concentration profiles (Rao et al., 2017).

In general, the low-Al CoCrFeNi-based high-entropy alloy shows striking phase stability during annealing at an elevated temperature after cold rolling for a long time. However,

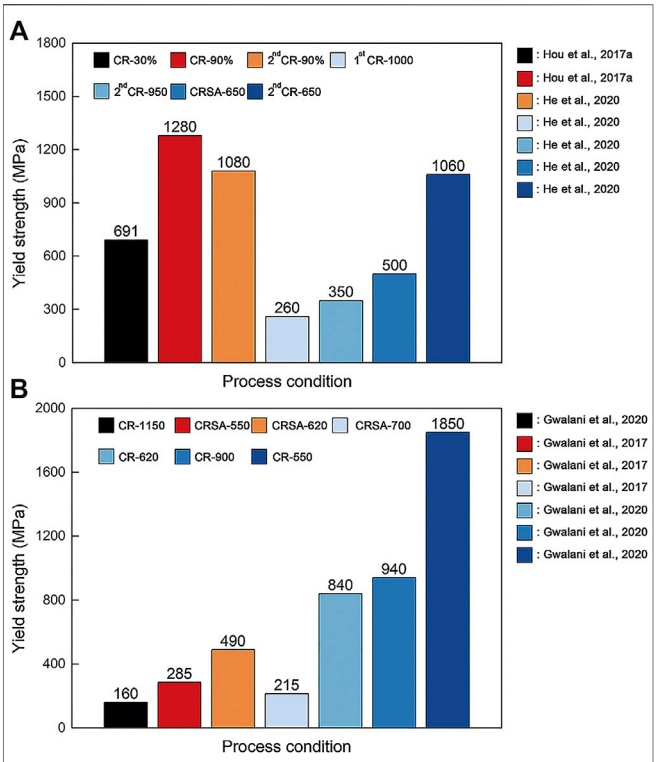

FIGURE 6 | Comparison of yield strength of **(A)** $Al_{0.25}CoCrFeNi$, and **(B)** $Al_{0.3}CoCrFeNi$ alloys under different thermal-mechanical processing conditions (Hou et al., 2017a; Gwalani et al., 2017; Gwalani et al., 2020; He et al., 2020).

intermediate temperature annealing for a long time could lead to phase decomposition and then form a dual-phase or tri-phase structure. During the thermo-mechanical processing of duplex $Al_xCoCrFeNi$ alloys, the fcc grains show slow growth during annealing for a long time, which is ascribed to the pinning effect resulting from the precipitated bcc phase in the grain boundaries. Besides, ordered phases are amenable to precipitation in fully recrystallized $Al_xCoCrFeNi$ alloys after a prolonged annealing time at an intermediated temperature. Prior deformation and subsequent annealing could substantially alter the morphology and distribution of precipitates. The dislocations introduced by pre-deformation could also act as heterogeneous nucleation sites for the secondary phase.

Mechanical Properties and Deformation Behavior

The tensile yield strength of the fcc-based $Al_{0.25}CoFeCrNi$ and $Al_{0.3}CoFeCrNi$ HEAs can be easily tuned via different thermal-mechanical processes, e.g., cold rolling and subsequent annealing (CRSA), as shown in **Figure 6** (Gwalani et al., 2017; Hou et al., 2017a; Gwalani et al., 2020; He et al., 2020). Hou et al. (2017a) carried out cold rolling processing on $Al_{0.25}CoFeCrNi$, resulting in a substantial strengthening of the alloy, with yield strength approaching 1,280 MPa (**Figure 6A**); however, this was at the expense of low ductility (ε ~2.3%). The annealing of the deformed alloy triggered recrystallization of the alloy, introducing an effective Hall-Petch strengthening (He et al., 2020). A further increase in YS could result from the precipitation of $L1_2$, B2, and/or σ nanoparticles. A high Hall-Petch strengthening, caused by direct annealing after deformation, led to a high yield strength (~1,060 MPa) with acceptable ductility (~19%) (**Figure 6A**). The increase in YS of the fully crystallized $Al_{0.3}CoFeCrNi$ alloy after the precipitation of the ordered phases is shown in **Figure 6B**, comparing the CR-1150, CRSA-550, CRSA-620, and CRSA-700 conditions. The combination of both the $L1_2$ and B2 type precipitates within the fcc matrix leading to optimal enhancement, with strengthening contributions calculated as ~126 MPa for the $L1_2$ precipitates, and ~56 MPa for the B2 precipitates, respectively (Gwalani et al., 2017). The multiple strengthening effects of grain boundary strengthening, composite reinforcement effect caused by ultrafine B2 and σ grains, and precipitation strengthening by Al–Ni rich nanoclusters give the CR-550 alloy high strength (~1,862 MPa) (Gwalani et al., 2020).

Grain Boundary Strengthening

With the grain refinement in $Al_{0.1}CoCrFeNi$ alloy twinning in recrystallized alloys could be severely inhibited, resulting in a lower value of strain hardening rate compared to as-cast alloy (Wu et al., 2019). The average grain size at a different scale (4.7, 7.5, 15.2, 32.5, and 59.5 μm) also affected the deformation behavior of the $Al_{0.1}CoCrFeNi$ alloy. The alloy with fine grains revealed a good balance of strength and ductility compared to those with coarse grain size. A mixed deformation mode of dislocation slip and twinning occurred in the alloys, certified by the high density of dislocation entanglements in association with the generation of deformation twin bundles (**Figures 7A–F–F**). However, more active twinning behavior was observed in coarse grain alloys with wider twin thickness and smaller twin spacing compared to the fine grain alloys during tensile deformation (**Figures 7G–I–I**), which promoted the hardening of the alloy and postponed the necking and thus enhanced the ductility (Yang et al., 2019c).

Liu et al. (2019a) fabricated an ultra fine grained triplex $Al_{0.3}CoCrFeNi$ high-entropy alloy through cold rolling and annealing at 700°C for 36 h. The alloy exhibited an extraordinary yield strength of 900 MPa and a total plastic strain of ~25%, as shown in **Figure 8A**. Grain boundary strengthening was calculated to be ~780 MPa, and the difference between the computed and experimental value of yield strength could be attributed to the fine B2 and σ precipitates that formed at the grain interior and boundaries during annealing treatment. The formation of extensive deformation nano twins during plastic deformation gave rise to the enhanced dislocation storage ability of the fcc phase and thus led to large ductility (**Figure 8B**). Even though the Hall–Petch strengthening contribution of $Al_{0.3}CoCrFeNi$ HEA increased from ~160 to ~850 MPa can be attributed to the extremely fine grains, the extent of Hall-Petch strengthening could nevertheless be reduced after the precipitation of the B2 and σ phases (Gwalani et al., 2020). These results indicate that subtle control of the grain size in high-entropy alloys is a strategy

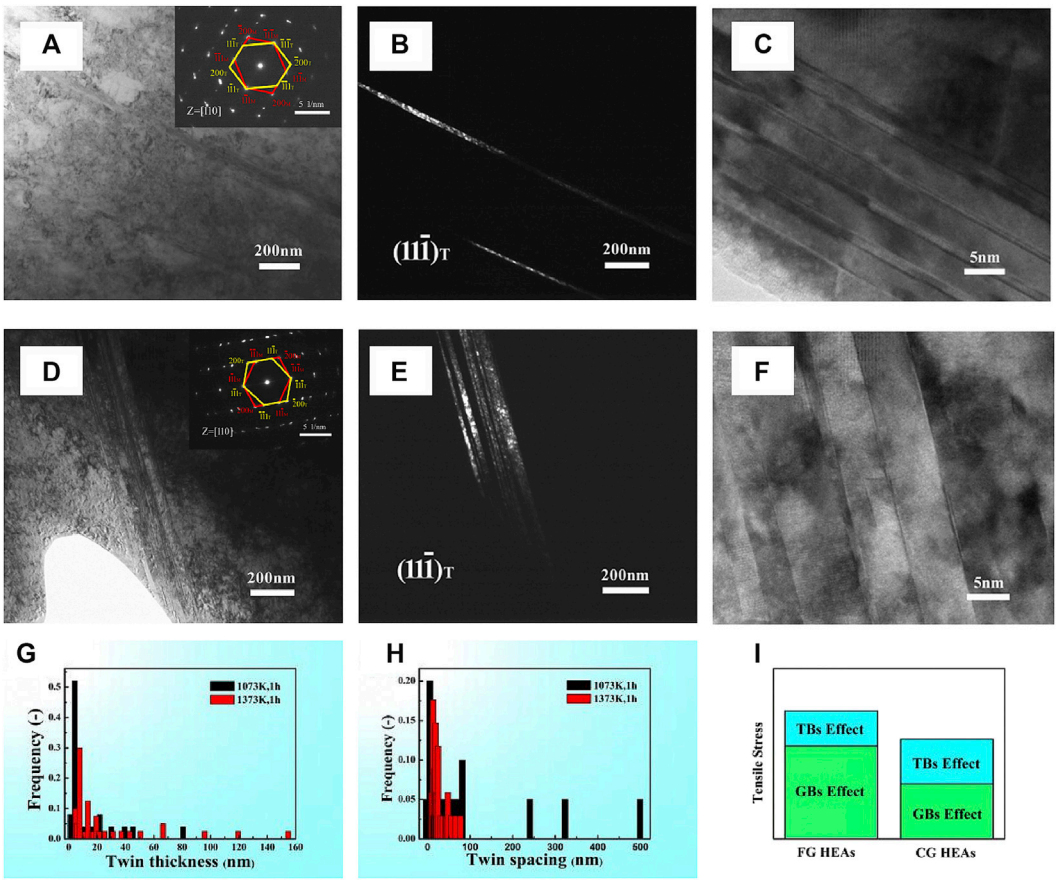

FIGURE 7 | (A) Bright-field (BF) image with corresponding selected-area diffraction pattern (SADP), **(B)** dark-field (DF) image, and **(C)** high-resolution TEM (HRTEM) image of FG (~4.7 μm) HEA, **(D)** BF image with corresponding SADP, **(E)** DF image, and **(F)** HRTEM image of CG (~59.5 μm) HEA; statistics of twin thickness **(G)**, and twin spacing **(H)**, **(I)** schematic illustrations of the contribution of twin boundaries (TBs) and grain boundaries (GBs) to the tensile stress of FG and CG HEAs (Yang et al., 2019c). (Reprinted from Journal of Alloys and Compounds, Vol 795, Yang et al., Revealing the Hall-Petch relationship of Al0.1CoCrFeNi high-entropy alloy and its deformation mechanisms, Pages No.272, Copyright (2019), with permission from Elsevier).

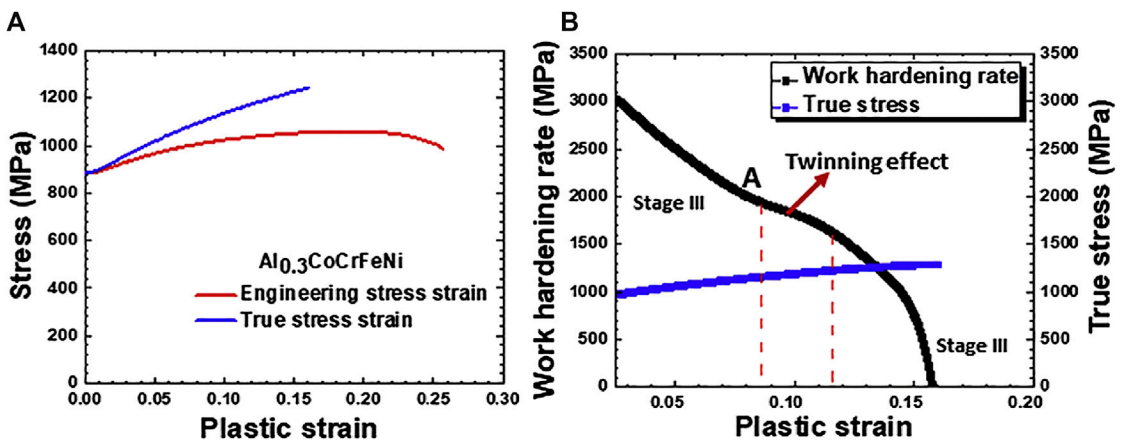

FIGURE 8 | Mechanical properties of UFG $Al_{0.3}CoCrFeNi$ **(A)** Engineering stress-strain and true stress-strain curves, and **(B)** work hardening rate true strain curve along with true stress-strain denoting the necking criterion (Liu et al., 2019a). (Reprinted from Scripta Materialia, Vol 158, Liu et al., NFatigue behavior of ultrafine grained triplex Al0.3CoCrFeNi high entropy alloy, Pages No.118, Copyright (2019), with permission from Elsevier).

of strengthening and toughening. However, the interplay of multiple strengthening mechanisms should also be taken into consideration to obtain the best performance.

Precipitation Strengthening

The fcc phase of $Al_{0.3}$CoCrFeNi alloy was transformed into an ordered B2 phase through tuning the cold rolling percentage and subsequently annealing at 800°C. The B2 grains acted as Eshelby type inclusion and could raise local stress levels during the deformation to trigger twinning (Choudhuri et al., 2018b). The yield strength of $Al_{0.3}$CoCrFeNi could be enhanced from ~260 to 490 MPa by introducing the γ' phase and grain boundary B2 phase. γ' precipitation led to a ~78% enhancement in YS while B2 precipitation led to a ~35% enhancement in YS (Gwalani et al., 2017). The boundaries of coherent nano-scaled $L1_2$ precipitate were inferred as thermal obstacles (Gangireddy et al., 2019). Introduction of the $L1_2$ precipitate effectively strengthened the dual-phase (fcc + B2) $Al_{0.7}$CoCrFeNi alloy and the strengthening contribution was modeled using Orowan bowing and by-pass mechanism (Gwalani et al., 2019).

Komarasamy et al. (2019) modified the hot-rolled $Al_{0.5}$CoCrFeNi alloy via high-temperature severe plastic deformation (HTSPD) and subsequent aging. The dissolution of the thermodynamically stable B2 phase during HTSPD then resulted in the precipitation of fine $L1_2$ and B2 phases as well as a thermodynamically unfavorable Al_3Ni phase, showing a combination of high ultimate tensile strength (1,400 MPa) and good elongation. Both the HTSPD and aged condition alloys with hierarchical microstructural features exhibited increasing strength and sustained work hardening, which were attributed to the precipitation of the thin B2 phase and increased dislocation storage caused by the Al_3Ni phase, respectively. It has been reported that the homogeneous distribution of the ordered $L1_2$ phase occurred at 650°C in fully-recrystallized $Al_{0.5}$CoCrFeNi alloy and that this can strengthen the fcc matrix by inducing substantial low-misfit nanoscale interfaces that resist dislocation motion effectively (Yang et al., 2019b). Heterogeneous plastic strain could accumulate near the fcc–bcc/B2 phase boundaries in Al-rich fcc-bcc Al_xCoCrFeNi HEAs. B2/bcc precipitates could prevent the formation of distinct deformation bands and their propagation in the fcc region of heat-treated $Al_{0.5}$CoCrFeNi alloy during room temperature deformation. The work hardening rate of the $Al_{0.5}$CoCrFeNi alloy proved to be high, and a large number of deformation twins were produced in the fcc matrix (Bonisch

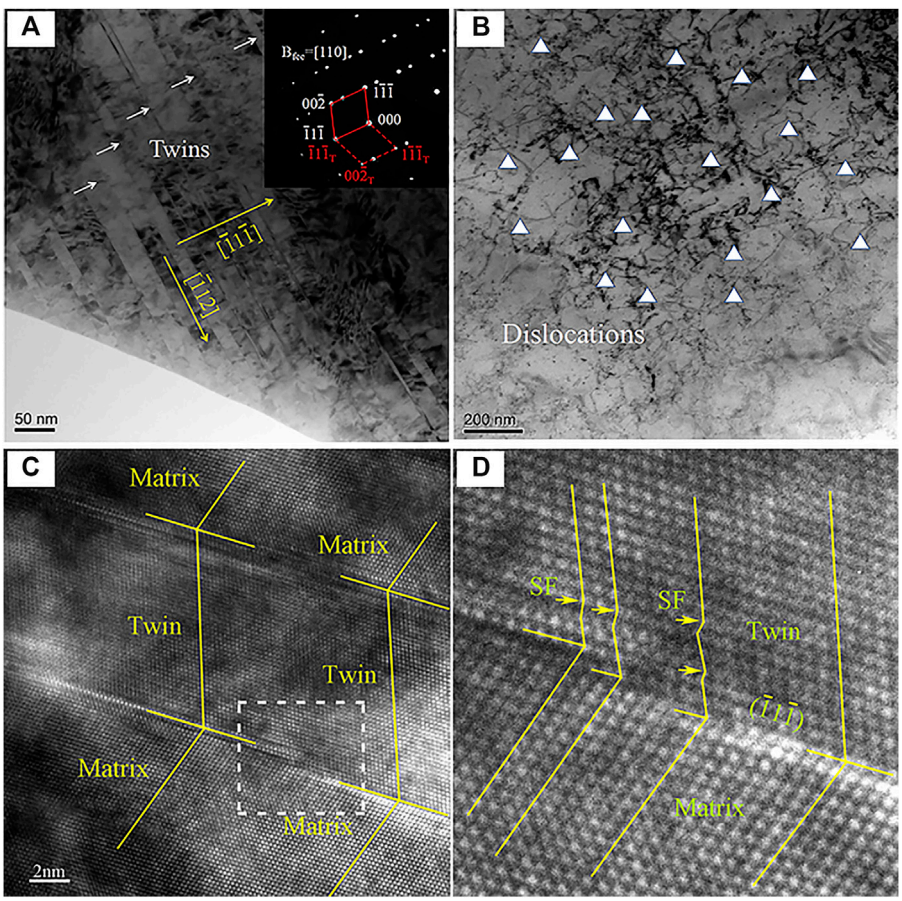

FIGURE 9 | Microstructure of $Al_{0.3}$CoCrFeNi HEA compressive samples **(A)** at 600°C, showing parallel nano-twins, **(B)** at 800°C, showing high density dislocations (Zhang et al., 2018). HETEM image of sample compressed at 600°C, **(C)** a typical deformation twin, and **(D)** the enlarged image of the white dashed square (Zhang et al., 2018).

et al., 2018). A large number of deformation twins generated by plastic deformation in hot-forged $Al_{0.7}$CoCrFeNi alloys could also be used for strengthening and toughing the alloy. However, when the volume fraction of the second phase exceeds a specific value, this could have a very obvious effect on the mechanical properties of the alloy, making it high strength but low plasticity.

In summary, it is interesting that the alloying of Al to fcc-based CoCrFeNi alloy could induce not only the transition from fcc to bcc but also fascinating phase transitions, including the ordering transition, bcc–hcp transition, and the formation of B2 and σ phases. Such phase transitions usually contribute to the substantial strengthening of the alloys. Synergy could be achieved in a variety of strengthening–toughening mechanisms through the appropriate thermal–mechanical process, which is expected to obtain the desired mechanical properties.

Deformation Behavior

Most of the fcc-based HEAs are reported to have rather low stacking fault energies (6–30 mJ/m^{-2}), and can form extensive twins during deformation at cryogenic temperature but minimal twinning at room temperature (Otto et al., 2013; Zhang et al., 2014; Choudhuri et al., 2019; Chen et al., 2020). For example, the $Al_{0.1}$CoCrFeNi alloy formed only a small fraction of nanoscale (~2 nm thick) deformation twins under quasistatic tension at room temperature, which provided an additional plastic deformation mode and improved the work hardening of the $Al_{0.1}$CoCrFeNi alloy (Choudhuri et al., 2018a). Deformation twins, as another fundamental plastic deformation mode, are relevant to internal and external factors such as crystal structure, strain rate, and temperature (Wang et al., 2018d). Severe plastic deformation could introduce higher internal stresses, which is expected to promote the emergence of deformation twins (Kumar et al., 2015; Choudhuri et al., 2018b; Chen et al., 2019). Choudhuri et al. (2019) investigated the deformation mechanisms of $Al_{0.3}$CoCrFeNi HEAs. TEM observation of the deformed behavior of the coarse-grained single-phase alloy indicated that the formation of the {111} slip band and generation of the nano-twin were the predominant deformation mechanisms. The presence of the hard B2 and σ intermetallics directly promoted the strain hardening of the fcc matrix phase. Within the fcc-B2 clusters, thicker deformation twins and dislocation plasticity were the main deformation mechanisms, while within the fcc-B2-σ clusters, dislocation plasticity, nano-twinning, plus limited crack formation in and around the σ grains were the primary deformation mechanisms.

Zhang et al. (2016) explored the hot deformation behavior of $Al_{0.5}$CrFeCoNi HEA in both the as-cast and homogenized conditions, where the flow stress heightened with increasing strain rate and lower temperature. Moreover, under the same deformation conditions, the flow stress in the homogenized state was higher than that in the as-cast state. The average activation energy was estimated to be ~300 KJ/mol. Serrations in flow behavior have also been reported for a few HEAs. Zhang et al. (2018) reported that an abnormal tendency happened in the serration curves during hot compression, indicating a conversion of the deformation mechanism at elevated temperatures. A large number of parallel deformation twins formed in the $Al_{0.3}$CoCrFeNi HEA after being compressed at 600°C, accounting for the continuous work-hardening phenomenon that occurred below 700°C (**Figures 9A,C,D**). As the temperature rose to 800°C, the escalation of dislocation mobility and SFE led to the transformation of the deformation mechanism from {111} <11–2> twinning to slip (**Figure 9B**). The transformation of the serration type was also reported in $Al_{0.5}$CrFeCoNi HEA (Niu et al., 2017b). With increasing temperature (200–500°C) and decreasing strain rate (10^{-3}–$10^{-}4\ s^{-1}$), the serration type changed from type A to type A+ B, and finally to type B+ C. The allow became brittle, which was attributed to dynamic strain aging since solute atoms could block the dislocation movement by interacting with dislocations.

CONCLUDING REMARKS

This article reviewed the effect of thermal-mechanical processes on Al_xCoCrFeNi high-entropy alloys, emphasizing the correlation of the microstructure and how this corresponds to mechanical performance. There is tremendous scope to further explore HEAs with hierarchical microstructure to achieve enhanced mechanical properties. By controlling the hierarchical grain structure or precipitation of various intermetallic compounds, the complex interplay of various strengthening mechanisms within the HEA results in a large range of strength-ductility combinations. However, such cumulative strengthening effects should be further systematically quantified. In addition, the temperature has a very significant impact on the stacking fault energy. Therefore, an alloy with relatively low stacking fault energy regulates the stacking fault energy, triggering the TWIP and trip effects of alloys, which is also expected to play a guiding role in further optimization of the strength and toughness of high-entropy alloy.

AUTHOR CONTRIBUTIONS

HY made a first draft, with substantial input, writing efforts, and discussions from JL, WW, HK, and JW.

FUNDING

This work was supported by the Natural Science Foundation of China (51774240 and 51571161), a fund from the State Key Laboratory of Solidification Processing in NWPU (2019-TS-04), the seed Foundation of Innovation and Creation for Graduate Students in Northwestern Polytechnical University (CX2020007), the Innovation Capability Support Program of Shaanxi (2020KJXX-073), the Natural Science Foundation of Chongqing (cstc2020jcyj-msxmX0976), and received Fundamental Research Funds for the Central Universities.

REFERENCES

Annasamy, M., Haghdadi, N., Taylor, A., Hodgson, P., and Fabijanic, D. (2019). Dynamic recrystallization behaviour of Al_xCoCrFeNi high entropy alloys during high-temperature plane strain compression. *Mater. Sci. Eng. A.* 745, 90–106. doi:10.1016/j.msea.2018.12.102

Bonisch, M., Wu, Y., and Sehitoglu, H. (2018). Twinning-induced strain hardening in dual-phase $FeCoCrNiAl_{0.5}$ at room and cryogenic temperature. *Sci. Rep.* 8, 10663. doi:10.1038/s41598-018-28784-1

Butler, T. M., and Weaver, M. L. (2017). Investigation of the phase stabilities in AlNiCoCrFe high entropy alloys. *J. Alloys Compd.* 691, 119–129. doi:10.1016/j.jallcom.2016.08.121

Cantor, B., Chang, I. T. H., Knight, P., and Vincent, A. J. B. (2004). Microstructural development in equiatomic multicomponent alloys. *Mater. Sci. Eng. A.* 375–377, 213–218

Cao, T., Shang, J., Zhao, J., Cheng, C., Wang, R., and Wang, H. (2016). The influence of Al elements on the structure and the creep behavior of Al_xCoCrFeNi high entropy alloys. *Mater. Lett.* 164, 344–347. doi:10.1016/j.matlet.2015.11.016

Chen, G., Li, L. T., Qiao, J. W., Jiao, Z. M., Ma, S. G., Ng, F. L., et al. (2019). Gradient hierarchical grain structures of $Al_{0.1}$CoCrFeNi high-entropy alloys through dynamic torsion. *Mater. Lett.* 238, 163–166. doi:10.1016/j.matlet.2018.11.176

Chen, S., Aitken, Z. H., Wu, Z., Yu, Z., Banerjee, R., and Zhang, Y. W. (2020). Hall-Petch and inverse Hall-Petch relations in high-entropy $CoNiFeAl_xCu_{1-x}$ alloys. *Mater. Sci. Eng. A.* 773. doi:10.1016/j.msea.2019.138873

Chen, T. K., Shun, T. T., Yeh, J. W., and Wong, M. S. (2004). Nanostructured nitride films of multi-element high-entropy alloys by reactive DC sputtering. *Surf. Coating. Technol.* 188-189, 193–200. doi:10.1016/j.surfcoat.2004.08.023

Chou, H. P., Chang, Y. S., Chen, S. K., and Yeh, J. W. (2009). Microstructure, thermophysical and electrical properties in Al_xCoCrFeNi ($0 \le x \le 2$) high-entropy alloys. *Mater. Sci. Eng. B.* 163, 184–189. doi:10.1016/j.mseb.2009.05.024

Choudhuri, D., Gwalani, B., Gorsse, S., Komarasamy, M., Mantri, S. A., Srinivasan, S. G., et al. (2019). Enhancing strength and strain hardenability via deformation twinning in fcc-based high entropy alloys reinforced with intermetallic compounds. *Acta Mater.* 165, 420–430. doi:10.1016/j.actamat.2018.12.010

Choudhuri, D., Komarasamy, M., Ageh, V., and Mishra, R. S. (2018a). Investigation of plastic deformation modes in $Al_{0.1}$CoCrFeNi high entropy alloy. *Mater. Chem. Phys.* 217, 308–314. doi:10.1016/j.matchemphys.2018.05.050

Choudhuri, D., Shukla, S., Green, W. B., Gwalani, B., Ageh, V., Banerjee, R., et al. (2018b). Crystallographically degenerate B2 precipitation in a plastically deformed fcc-based complex concentrated alloy. *Mater. Res. Lett.* 6, 171–177. doi:10.1080/21663831.2018.1426649

Cieslak, J., Tobola, J., Berent, K., and Marciszko, M. (2018). Phase composition of Al_xFeNiCrCo high entropy alloys prepared by sintering and arc-melting methods. *J. Alloys Compd.* 740, 264–272. doi:10.1016/j.jallcom.2017.12.333

Du, X. H., Li, W. P., Chang, H. T., Yang, T., Duan, G. S., Wu, B. L., et al. (2020). Dual heterogeneous structures lead to ultrahigh strength and uniform ductility in a Co-Cr-Ni medium-entropy alloy. *Nat. Commun.* 11, 2390. doi:10.1038/s41467-020-16085-z

Gangireddy, S., Gwalani, B., and Mishra, R. S. (2018a). Grain size dependence of strain rate sensitivity in a single phase FCC high entropy alloy Al0. 3CoCrFeNi. *Mater. Sci. Eng. A.* 736, 344–348. doi:10.1016/j.msea.2018.09.009

Gangireddy, S., Gwalani, B., Soni, V., Banerjee, R., and Mishra, R. S. (2019). Contrasting mechanical behavior in precipitation hardenable Al_xCoCrFeNi high entropy alloy microstructures: single phase FCC vs. dual phase FCC–BCC. *Mater. Sci. Eng. A.* 739, 158–166. doi:10.1016/j.msea.2018.10.021

Gangireddy, S., Kaimiao, L., Gwalani, B., and Mishra, R. (2018b). Microstructural dependence of strain rate sensitivity in thermomechanically processed $Al_{0.1}$CoCrFeNi high entropy alloy. *Mater. Sci. Eng. A.* 727, 148–159. doi:10.1016/j.msea.2018.04.108

Gao, X., Lu, Y., Liu, J., Wang, J., Wang, T., and Zhao, Y. (2019). Extraordinary ductility and strain hardening of $Cr_{26}Mn_{20}Fe_{20}Co_{20}Ni_{14}$ TWIP high-entropy alloy by cooperative planar slipping and twinning. *Materialia.* 8, 21–78. doi:10.1016/j.mtla.2019.100485

Garlapati, M. M., Vaidya, M., Karati, A., Mishra, S., Bhattacharya, R., and Murty, B. S. (2020). Influence of Al content on thermal stability of nanocrystalline Al_xCoCrFeNi high entropy alloys at low and intermediate temperatures. *Adv. Powder Technol.* 7, 33–68. doi:10.1016/j.apt.2020.02.032

George, E. P., Curtin, W. A., and Tasan, C. C. (2020). High entropy alloys: a focused review of mechanical properties and deformation mechanisms. *Acta Mater.* 188, 435–474. doi:10.1016/j.actamat.2019.12.015

Gorsse, S., Miracle, D. B., and Senkov, O. N. (2017). Mapping the world of complex concentrated alloys. *Acta Mater.* 135, 177–187. doi:10.1016/j.actamat.2017.06.027

Guillot, I., Tyrman, M., Perrière, L., Couzinié, J. P. P., Lilensten, L., Prima, F., et al. (2020). Ultrafine-grained two-phase high-entropy alloy microstructures obtained via recrystallization: mechanical properties. *Front. Mater.* 8, 221–288. doi:10.3389/fmats.2020.00125

Guo, S., Ng, C., and Liu, C. T. (2013). Anomalous solidification microstructures in Co-free Al_xCrCuFeNi$_2$ high-entropy alloys. *J. Alloys Compd.* 557, 77–81. doi:10.1016/j.jallcom.2013.01.007

Guo, T., Li, J., Wang, J., Wang, W. Y., Liu, Y., Luo, X., et al. (2018). Microstructure and properties of bulk $Al_{0.5}$CoCrFeNi high-entropy alloy by cold rolling and subsequent annealing. *Mater. Sci. Eng. A.* 729, 141–148. doi:10.1016/j.msea.2018.05.054

Guo, T., Li, J., Wang, J., Wang, Y., Kou, H., and Niu, S. (2017). Liquid-phase separation in undercooled CoCrCuFeNi high entropy alloy. *Intermetallics.* 86, 110–115. doi:10.1016/j.intermet.2017.03.021

Gwalani, B., Choudhuri, D., Liu, K., Lloyd, J. T., Mishra, R. S., and Banerjee, R. (2020). Interplay between single phase solid solution strengthening and multi-phase strengthening in the same high entropy alloy. *Mater. Sci. Eng. A.* 771, 437–515. doi:10.1016/j.msea.2019.138620

Gwalani, B., Gangireddy, S., Zheng, Y., Soni, V., Mishra, R. S., and Banerjee, R. (2019). Influence of ordered $L1_2$ precipitation on strain-rate dependent mechanical behavior in a eutectic high entropy alloy. *Sci. Rep.* 9, 6371. doi:10.1038/s41598-019-42870-y

Gwalani, B., Gorsse, S., Choudhuri, D., Styles, M., Zheng, Y., Mishra, R. S., et al. (2018). Modifying transformation pathways in high entropy alloys or complex concentrated alloys via thermo-mechanical processing. *Acta Mater.* 153, 169–185. doi:10.1016/j.actamat.2018.05.009

Gwalani, B., Soni, V., Lee, M., Mantri, S. A., Ren, Y., and Banerjee, R. (2017). Optimizing the coupled effects of Hall–Petch and precipitation strengthening in a $Al_{0.3}$CoCrFeNi high entropy alloy. *Mater. Des.* 121, 254–260. doi:10.1016/j.matdes.2017.02.072

Haghdadi, N., Primig, S., Annasamy, M., Cizek, P., Hodgson, P. D., and Fabijanic, D. M. (2020a). Dynamic recrystallization in Al_xCoCrFeNi duplex high entropy alloys. *J. Alloys Compd.* 830, 115–233. doi:10.1016/j.jallcom.2020.154720

Haghdadi, N., Primig, S., Annasamy, M., Cizek, P., Hodgson, P. D., and Fabijanic, D. M. (2020b). On the hot-worked microstructure of a face-centered cubic $Al_{0.3}$CoCrFeNi high entropy alloy. *Scripta Mater.* 178, 144–149. doi:10.1016/j.scriptamat.2019.11.022

He, F., Wang, Z., Wu, Q., Li, J., Wang, J., and Liu, C. T. (2017). Phase separation of metastable CoCrFeNi high entropy alloy at intermediate temperatures. *Scripta Mater.* 126, 15–19. doi:10.1016/j.scriptamat.2016.08.008

He, J. Y., Wang, H., Huang, H. L., Xu, X. D., Chen, M. W., Wu, Y., et al. (2016a). A precipitation-hardened high-entropy alloy with outstanding tensile properties. *Acta Mater.* 102, 187–196. doi:10.1016/j.actamat.2015.08.076

He, J. Y., Wang, H., Wu, Y., Liu, X. J., Mao, H. H., Nieh, T. G., et al. (2016b). Precipitation behavior and its effects on tensile properties of FeCoNiCr high-entropy alloys. *Intermetallics.* 79, 41–52. doi:10.1016/j.intermet.2016.09.005

He, Y., Yang, H., Zhao, C., Zhang, Y., Pan, X., Li, J., et al. (2020). Enhancing mechanical properties of $Al_{0.25}$CoCrFeNi high-entropy alloy via cold rolling and subsequent annealing. *J. Alloys Compd.* 830, 23–45. doi:10.1016/j.jallcom.2020.154645

Hou, J., Shi, X., Qiao, J., Zhang, Y., Liaw, P. K., and Wu, Y. (2019). Ultrafine-grained dual phase $Al_{0.45}$CoCrFeNi high-entropy alloys. *Mater. Des.* 180, 107910. doi:10.1016/j.matdes.2019.107910

Hou, J., Zhang, M., Ma, S., Liaw, P. K., Zhang, Y., and Qiao, J. (2017a). Strengthening in $Al_{0.25}$CoCrFeNi high-entropy alloys by cold rolling. *Mater. Sci. Eng. A.* 707, 593–601. doi:10.1016/j.msea.2017.09.089

Hou, J., Zhang, M., Yang, H., and Qiao, J. (2017b). Deformation behavior of $Al_{0.25}$CoCrFeNi high-entropy alloy after recrystallization. *Metals.* 7, 12–23. doi:10.3390/met7040111

Jasiewicz, K., Cieslak, J., Kaprzyk, S., and Tobola, J. (2015). Relative crystal stability of Al_xFeNiCrCo high entropy alloys from XRD analysis and formation energy calculation. *J. Alloys Compd.* 648, 307–312. doi:10.1016/j.jallcom.2015.06.260

Juan, C. C., Hsu, C. Y., Tsai, C. W., Wang, W. R., Sheu, T. S., Yeh, J. W., et al. (2013). On microstructure and mechanical performance of $AlCoCrFeMo_{0.5}Ni_x$ high-entropy alloys. *Intermetallics.* 32, 401–407. doi:10.1016/j.intermet.2012.09.008

Kao, Y. F., Chen, S. K., Chen, T. J., Chu, P. C., Yeh, J. W., and Lin, S. J. (2011). Electrical, magnetic, and Hall properties of Al_xCoCrFeNi high-entropy alloys. *J. Alloys Compd.* 509, 1607–1614. doi:10.1016/j.jallcom.2010.10.210

Kao, Y. F., Chen, T. J., Chen, S. K., and Yeh, J. W. (2009). Microstructure and mechanical property of as-cast, -homogenized, and -deformed Al_xCoCrFeNi ($0 \le x \le 2$) high-entropy alloys. *J. Alloys Compd.* 488, 57–64. doi:10.1016/j.jallcom.2009.08.090

Kireeva, I. V., Chumlyakov, Y. I., Pobedennaya, Z. V., and Vyrodova, A. V. (2020). Effect of γ′-phase particles on the orientation and temperature dependence of the mechanical behaviour of $Al_{0.3}$CoCrFeNi high-entropy alloy single crystals. *Mater. Sci. Eng. A.* 772. doi:10.1016/j.msea.2019.138772

Komarasamy, M., Wang, T., Liu, K., Reza-Nieto, L., and Mishra, R. S. (2019). Hierarchical multi-phase microstructural architecture for exceptional strength-ductility combination in a complex concentrated alloy via high-temperature severe plastic deformation. *Scripta Mater.* 162, 38–43. doi:10.1016/j.scriptamat.2018.10.033

Kumar, N., Ying, Q., Nie, X., Mishra, R. S., Tang, Z., Liaw, P. K., et al. (2015). High strain-rate compressive deformation behavior of the $Al_{0.1}$CrFeCoNi high entropy alloy. *Mater. Des.* 86, 598–602. doi:10.1016/j.matdes.2015.07.161

Li, C., Li, J. C., Zhao, M., and Jiang, Q. (2009). Effect of alloying elements on microstructure and properties of multiprincipal elements high-entropy alloys. *J. Alloys Compd.* 475, 752–757. doi:10.1016/j.jallcom.2008.07.124

Li, D., and Zhang, Y. (2016). The ultrahigh charpy impact toughness of forged Al_xCoCrFeNi high entropy alloys at room and cryogenic temperatures. *Intermetallics.* 70, 24–28. doi:10.1016/j.intermet.2015.11.002

Li, J., Jia, W., Wang, J., Kou, H., Zhang, D., and Beaugnon, E. (2016). Enhanced mechanical properties of a CoCrFeNi high entropy alloy by supercooling method. *Mater. Des.* 95, 183–187. doi:10.1016/j.matdes.2016.01.112

Li, Q., Zhang, T. W., Qiao, J. W., Ma, S. G., Zhao, D., Lu, P., et al. (2019). Mechanical properties and deformatiikon behavior of dual-phase $Al_{0.6}$CoCrFeNi high-entropy alloys with heterogeneous structure at room and cryogenic temperatures. *J. Alloys Compd.* 95, 152663. doi:10.1016/j.jallcom.2019.152663

Liu, G., Liu, L., Liu, X., Wang, Z., Han, Z., Zhang, G., et al. (2018). Microstructure and mechanical properties of $Al_{0.7}$CoCrFeNi high-entropy-alloy prepared by directional solidification. *Intermetallics.* 93, 93–100. doi:10.1016/j.intermet.2017.11.019

Liu, K., Komarasamy, M., Gwalani, B., Shukla, S., and Mishra, R. S. (2019a). Fatigue behavior of ultrafine grained triplex $Al_{0.3}$CoCrFeNi high entropy alloy. *Scripta Mater.* 158, 116–120. doi:10.1016/j.scriptamat.2018.08.048

Liu, W. H., Lu, Z. P., He, J. Y., Luan, J. H., Wang, Z. J., Liu, B., et al. (2016). Ductile $CoCrFeNiMo_x$ high entropy alloys strengthened by hard intermetallic phases. *Acta Mater.* 116, 332–342 doi:10.1016/j.actamat.2016.06.063

Liu, W. H., Wu, Y., He, J. Y., Zhang, Y., Liu, C. T., and Lu, Z. P. (2014). The phase competition and stability of high-entropy alloys. *J. Occup. Med.* 66, 1973–1983. doi:10.1016/j.actamat.2016.06.063

Liu, Y. Y., Chen, Z., Shi, J. C., Wang, Z. Y., and Zhang, J. Y. (2019b). The effect of Al content on microstructures and comprehensive properties in Al_xCoCrCuFeNi high entropy alloys. *Vacuum.* 161, 143–149. doi:10.1016/j.vacuum.2018.12.009

Lu, K. (2016). Stabilizing nanostructures in metals using grain and twin boundary architectures. *Nature Reviews Materials.* 1, 16019. doi:10.1038/natrevmats.2016.19

Lu, Y., Dong, Y., Guo, S., Jiang, L., Kang, H., Wang, T., et al. (2014). A promising new class of high-temperature alloys: eutectic high-entropy alloys. *Sci. Rep.* 4, 33–79. doi:10.1038/srep06200

Lu, Y., Gao, X., Dong, Y., Wang, T., Chen, H. L., Maob, H., et al. (2018). Preparing bulk ultrafine-microstructure high-entropy alloys via direct solidification. *Nanoscale.* 10, 1912–1919. doi:10.1039/C7NR07281C

Lu, Y., Gao, X., Jiang, L., Chen, Z., Wang, T., Jie, J., et al. (2017). Directly cast bulk eutectic and near-eutectic high entropy alloys with balanced strength and ductility in a wide temperature range. *Acta Mater.* 124, 143–150. doi:10.1016/j.actamat.2016.11.016

Ma, S. G., Liaw, P. K., Gao, M. C., Qiao, J. W., Wang, Z. H., and Zhang, Y. (2014). Damping behavior of Al_xCoCrFeNi high-entropy alloys by a dynamic mechanical analyzer. *J. Alloys Compd.* 604, 331–339. doi:10.1016/j.jallcom.2014.03.050

Macdonald, B. E., Fu, Z., Wang, X., Li, Z., Chen, W., Zhou, Y., et al. (2019). Influence of phase decomposition on mechanical behavior of an equiatomic CoCuFeMnNi high entropy alloy. *Acta Mater.* 181, 25–35. doi:10.1016/j.actamat.2019.09.030

Miracle, D. B. (2015). Critical Assessment 14: high entropy alloys and their development as structural materials. *Mater. Sci. Technol.* 31, 1142–1147. doi:10.1179/1743284714y.0000000749

Munitz, A., Salhov, S., Hayun, S., and Frage, N. (2016). Heat treatment impacts the micro-structure and mechanical properties of AlCoCrFeNi high entropy alloy. *J. Alloys Compd.* 683, 221–230. doi:10.1016/j.jallcom.2016.05.034

Nartu, M. S. K. K. Y., Alam, T., Dasari, S., Mantri, S. A., Gorsse, S., Siller, H., et al. (2020). Enhanced tensile yield strength in laser additively manufactured $Al_{0.3}$CoCrFeNi high entropy alloy. *Materialia.* 9, 329–447. doi:10.1016/j.mtla.2019.100522

Niu, S., Kou, H., Guo, T., Zhang, Y., Wang, J., and Li, J. (2016). Strengthening of nanoprecipitations in an annealed $Al_{0.5}$CoCrFeNi high entropy alloy. *Mater. Sci. Eng. A.* 671, 82–86. doi:10.1016/j.msea.2016.06.040

Niu, S., Kou, H., Zhang, Y., Wang, J., and Li, J. (2017b). The characteristics of serration in $Al_{0.5}$CoCrFeNi high entropy alloy. *Mater. Sci. Eng. A.* 702, 96–103. doi:10.1016/j.msea.2017.05.075

Niu, S. Z., Kou, H. C., Wang, J., and Li, J. S. (2017a). Improved tensile properties of $Al_{0.5}$CoCrFeNi high-entropy alloy by tailoring microstructures. *Rare Metals.* 12, 69–119. doi:10.1007/s12598-016-0860-y

Ogura, M., Fukushima, T., Zeller, R., and Dederichs, P. H. (2017). Structure of the high-entropy alloy AlCrFeCoNi: fcc versus bcc. *J. Alloys Compd.* 715, 454–459. doi:10.1016/j.jallcom.2017.04.318

Otto, F., Yang, Y., Bei, H., and George, E. P. (2013). Relative effects of enthalpy and entropy on the phase stability of equiatomic high-entropy alloys. *Acta Mater.* 61, 2628–2638. doi:10.1016/j.actamat.2013.01.042

Rao, J. C., Diao, H. Y., Ocelík, V., Vainchtein, D., Zhang, C., Kuo, C., et al. (2017). Secondary phases in Al_xCoCrFeNi high-entropy alloys: an *in-situ* TEM heating study and thermodynamic appraisal. *Acta Mater.* 131, 206–220. doi:10.1016/j.actamat.2017.03.066

Rao, J. C., Ocelík, V., Vainchtein, D., Tang, Z., Liaw, P. K., and De Hosson, J. T. M. (2016). The fcc-bcc crystallographic orientation relationship in Al_xCoCrFeNi high-entropy alloys. *Mater. Lett.* 176, 29–32. doi:10.1016/j.matlet.2016.04.086

Schneider, M., George, E. P., Manescau, T. J., Záležák, T., Hunfeld, J., Dlouhý, A., et al. (2020). Analysis of strengthening due to grain boundaries and annealing twin boundaries in the CrCoNi medium-entropy alloy. *Int. J. Plast.* 124, 155–169. doi:10.1016/j.ijplas.2019.08.009

Senkov, O. N., Miller, J. D., Miracle, D. B., and Woodward, C. (2015). Accelerated exploration of multi-principal element alloys with solid solution phases. *Nat. Commun.* 6, 6529. doi:10.1038/ncomms7529

Shi, Y., Collins, L., Feng, R., Zhang, C., Balke, N., Liaw, P. K., et al. (2018). Homogenization of Al_xCoCrFeNi high-entropy alloys with improved corrosion resistance. *Corrosion Sci.* 133, 120–131. doi:10.1016/j.corsci.2018.01.030

Sriharitha, R., Murty, B. S., and Kottada, R. S. (2013). Phase formation in mechanically alloyed Al_xCoCrCuFeNi (x = 0.45, 1, 2.5, 5 mol) high entropy alloys. *Intermetallics.* 32, 119–126. doi:10.1016/j.intermet.2012.08.015

Stepanov, N. D., Shaysultanov, D. G., Salishchev, G. A., Tikhonovsky, M. A., Oleynik, E. E., Tortika, A. S., et al. (2015). Effect of V content on microstructure and mechanical properties of the $CoCrFeMnNiV_x$ high entropy alloys. *J. Alloys Compd.* 628, 170–185. doi:10.1016/j.jallcom.2014.12.157

Sun, S. J., Tian, Y. Z., An, X. H., Lin, H. R., Wang, J. W., and Zhang, Z. F. (2018). Ultrahigh cryogenic strength and exceptional ductility in ultrafine-grained

CoCrFeMnNi high-entropy alloy with fully recrystallized structure. *Mater. Today Nano.* 4, 46–53. doi:10.1016/j.mtnano.2018.12.002

Tan, Y., Li, J., Tang, Z., Wang, J., and Kou, H. (2018a). Design of high-entropy alloys with a single solid-solution phase: average properties vs. their variances. *J. Alloys Compd.* 742, 430–441. doi:10.1016/j.jallcom.2018.01.252

Tan, Y., Li, J., Wang, J., Kolbe, M., and Kou, H. (2018b). Microstructure characterization of CoCrFeNiMnPd eutectic high-entropy alloys. *J. Alloys Compd.* 731, 600–611. doi:10.1016/j.jallcom.2017.09.057

Tan, Y., Li, J., Wang, J., and Kou, H. (2019). Effect of Mn addition on the microstructures and mechanical properties of CoCrFeNiPd high entropy alloy. *Entropy.* 21, 153–241. doi:10.3390/e21030288

Tan, Y., Li, J., Wang, J., and Kou, H. (2017). Seaweed eutectic-dendritic solidification pattern in a CoCrFeNiMnPd eutectic high-entropy alloy. *Intermetallics.* 85, 74–79. doi:10.1016/j.intermet.2017.02.004

Tang, Q., Huang, Y., Cheng, H., Liao, X., Langdon, T. G., and Dai, P. (2016). The effect of grain size on the annealing-induced phase transformation in an $Al_{0.3}$CoCrFeNi high entropy alloy. *Mater. Des.* 105, 381–385. doi:10.1016/j.matdes.2016.05.079

Tong, C. J., Chen, M. R., Yeh, J. W., Lin, S. J., Chen, S. K., Shun, T. T., et al. (2005a). Mechanical performance of the Al_xCoCrCuFeNi high-entropy alloy system with multiprincipal elements. *Metall. Mater. Trans.* 36, 1263–1271. doi:10.1007/s11661-005-0218-9

Tong, C. J., Chen, Y. L., Yeh, J. W., Lin, S. J., Chen, S. K., Shun, T. T., et al. (2005b). Microstructure characterization of Al_xCoCrCuFeNi high-entropy alloy system with multiprincipal elements. *Metall. Mater. Trans.* 36, 881–893. doi:10.1007/s11661-005-0283-0

Tong, Y., Chen, D., Han, B., Wang, J., Feng, R., Yang, T., et al. (2019). Outstanding tensile properties of a precipitation-strengthened $FeCoNiCrTi_{0.2}$ high-entropy alloy at room and cryogenic temperatures. *Acta Mater.* 165, 228–240. doi:10.1016/j.actamat.2018.11.049

Troparevsky, M. C., Morris, J. R., Kent, P. R. C., Lupini, A. R., and Stocks, G. M. (2015). Criteria for predicting the formation of single-phase high-entropy alloys. *Phys. Rev. X.* 5, 114. doi:10.1103/PhysRevX.5.011041

Tung, C. C., Yeh, J. W., Shun, T. T., Chen, S. K., Huang, Y. S., and Chen, H. C. (2007). On the elemental effect of AlCoCrCuFeNi high-entropy alloy system. *Mater. Lett.* 61, 1–5. doi:10.1016/j.matlet.2006.03.140

Wang, C., Li, X., Li, Z., Wang, Q., Zheng, Y., Ma, Y., et al. (2020). The resistivity–temperature behavior of Al_xCoCrFeNi high-entropy alloy films. *Thin Solid Films.* 700. doi:10.1016/j.tsf.2020.137895

Wang, J., Li, J., Wang, J., Bu, F., Kou, H., Li, C., et al. (2018a). Effect of solidification on microstructure and properties of $FeCoNi(AlSi)_{0.2}$ high-entropy alloy under strong static magnetic field. *Entropy.* 20, 773–779. doi:10.3390/e20040275

Wang, J., Niu, S., Guo, T., Kou, H., and Li, J. (2017a). The FCC to BCC phase transformation kinetics in an $Al_{0.5}$CoCrFeNi high entropy alloy. *J. Alloys Compd.* 710, 144–150. doi:10.1016/j.jallcom.2017.03.249

Wang, J., Wei, C., Yang, H., Guo, T., Xu, T., and Li, J. (2018b). Phase transformation kinetics of a FCC Al0.25CoCrFeNi high-entropy alloy during isochronal heating. *Metals.* 8, 283–289. doi:10.3390/met8121015

Wang, J., Yang, H., Guo, T., Wang, J., Wang, W. Y., and Li, J. (2018c). Effect of cold rolling on the phase transformation kinetics of an $Al_{0.5}$CoCrFeNi high-entropy alloy. *Entropy.* 20, 63–95. doi:10.3390/e20120917

Wang, J., Zhang, Y., Niu, S. Z., Wang, W. Y., Kou, H. C., Li, J. S., et al. (2017b). Formation of a hexagonal closed-packed phase in $Al_{0.5}$CoCrFeNi high entropy alloy. *MRS Communications.* 7, 879–884. doi:10.1557/mrc.2017.109

Wang, J., Zhang, Y., Xiao, H., Li, L., Kou, H., and Li, J. (2019a). A novel strategy for enhancing mechanical performance of $Al_{0.5}$CoCrFeNi high-entropy alloy via high magnetic field. *Mater. Lett.* 240, 250–252. doi:10.1016/j.matlet.2018.12.127

Wang, L., Qiao, J. W., Ma, S. G., Jiao, Z. M., Zhang, T. W., Chen, G., et al. (2018d). Mechanical response and deformation behavior of $Al_{0.6}$CoCrFeNi high-entropy alloys upon dynamic loading. *Mater. Sci. Eng. A.* 727, 208–213. doi:10.1016/j.msea.2018.05.001

Wang, W. R., Wang, W. L., Wang, S. C., Tsai, Y. C., Lai, C. H., and Yeh, J. W. (2012). Effects of Al addition on the microstructure and mechanical property of Al_xCoCrFeNi high-entropy alloys. *Intermetallics.* 26, 44–51. doi:10.1016/j.intermet.2012.03.005

Wang, W. R., Wang, W. L., and Yeh, J. W. (2014). Phases, microstructure and mechanical properties of Al_xCoCrFeNi high-entropy alloys at elevated temperatures. *J. Alloys Compd.* 589, 143–152. doi:10.1016/j.jallcom.2013.11.084

Wang, W. Y., Wang, J., Lin, D., Zou, C., Wu, Y., Hu, Y., et al. (2017c). Revealing the microstates of body-centered-cubic (BCC) equiatomic high entropy alloys. *J. Phase Equilibria Diffus.* 38, 404–415. doi:10.1007/s11669-017-0565-4

Wang, X., Zhou, W., Liu, P., Song, S., and Reddy, K. M. (2019b). Atomic scale structural characterization of B2 phase precipitated along FCC twin boundary in a $CoCrFeNiAl_{0.3}$ high entropy alloy. *Scripta Mater.* 162, 161–165. doi:10.1016/j.scriptamat.2018.11.016

Wang, Y. P., Li, B. S., Ren, M. X., Yang, C., and Fu, H. Z. (2008). Microstructure and compressive properties of AlCrFeCoNi high entropy alloy. *Mater. Sci. Eng. A.* 491, 154–158. doi:10.1016/j.msea.2008.01.064

Wani, I. S., Bhattacharjee, T., Sheikh, S., Lu, Y. P., Chatterjee, S., Bhattacharjee, P. P., et al. (2016). Ultrafine-grained $AlCoCrFeNi_{2.1}$ eutectic high-entropy alloy. *Materials Research Letters.* 4, 174–179. doi:10.1080/21663831.2016.1160451

Wu, J. M., Lin, S. J., Yeh, J. W., Chen, S. K., Huang, Y. S., and Chen, H. C. (2006). Adhesive wear behavior of Al_xCoCrCuFeNi high-entropy alloys as a function of aluminum content. *Wear.* 261, 513–519. doi:10.1016/j.wear.2005.12.008

Wu, S. W., Wang, G., Wang, Q., Jia, Y. D., Yi, J., Zhai, Q. J., et al. (2019). Enhancement of strength-ductility trade-off in a high-entropy alloy through a heterogeneous structure. *Acta Mater.* 165, 444–458. doi:10.1016/j.actamat.2018.12.012

Xia, S., Gao, M. C., Yang, T., Liaw, P. K., and Zhang, Y. (2016). Phase stability and microstructures of high entropy alloys ion irradiated to high doses. *J. Nucl. Mater.* 480, 100–108. doi:10.1016/j.jnucmat.2016.08.017

Xia, S. Q., Gao, M. C., and Zhang, Y. (2018). Abnormal temperature dependence of impact toughness in Al_xCoCrFeNi system high entropy alloys. *Mater. Chem. Phys.* 210, 213–221. doi:10.1016/j.jnucmat.2016.08.017

Yang, H., Li, J., Guo, T., Wang, W. Y., Kou, H., and Wang, J. (2019b). Fully recrystallized $Al_{0.5}$CoCrFeNi high-entropy alloy strengthened by nanoscale precipitates. *Met. Mater. Int.* 25, 1145–1150. doi:10.1007/s12540-019-00284-5

Yang, H., Li, J., Pan, X., Wang, W. Y., Kou, H., and Wang, J. (2020). Nanophase precipitation and strengthening in a dual-phase $Al_{0.5}$CoCrFeNi high-entropy alloy. *J. Mater. Sci. Technol.* 72, 1–7. doi:10.1016/j.jmst.2020.02.069

Yang, H. X., Li, J. S., Guo, T., Wang, W. Y., Kou, H. C., and Wang, J. (2019a). Evolution of microstructure and hardness in a dual-phase $Al_{0.5}$CoCrFeNi high-entropy alloy with different grain sizes. *Rare Metals.* 39, 156–161. doi:10.1007/s12598-019-01320-4

Yang, J., Qiao, J. W., Ma, S. G., Wu, G. Y., Zhao, D., and Wang, Z. H. (2019c). Revealing the Hall-Petch relationship of $Al_{0.1}$CoCrFeNi high-entropy alloy and its deformation mechanisms. *J. Alloys Compd.* 795, 269–274. doi:10.1016/j.jallcom.2019.04.333

Yeh, J. W., Chen, S. K., Lin, S. J., Gan, J. Y., Chin, T. S., Shun, T. T., et al. (2004). Nanostructured high-entropy alloys with multiple principal elements: novel alloy design concepts and outcomes. *Adv. Eng. Mater.* 6, 299–303. doi:10.1002/adem.200300567

Yu, H., Fang, W., Chang, R., Bai, X., Zhang, X., Liu, B., et al. (2020). Effects of annealing temperature and cooling medium on the microstructure and mechanical properties of a novel dual phase high entropy alloy. *Mater. Char.* 163. doi:10.1016/j.matchar.2020.110291

Yu, P. F., Cheng, H., Zhang, L. J., Zhang, H., Jing, Q., Ma, M. Z., et al. (2016). Effects of high pressure torsion on microstructures and properties of an $Al_{0.1}$CoCrFeNi high-entropy alloy. *Mater. Sci. Eng. A.* 655, 283–291. doi:10.1016/j.msea.2015.12.085

Yuan, Y., Wu, Y., Tong, X., Zhang, H., Wang, H., Liu, X. J., et al. (2017). Rare-earth high-entropy alloys with giant magnetocaloric effect. *Acta Mater.* 125, 481–489. doi:10.1016/j.actamat.2016.12.021

Zhang, F., Wu, Y., Lou, H., Zeng, Z., Prakapenka, V. B., Greenberg, E., et al. (2017). Polymorphism in a high-entropy alloy. *Nat. Commun.* 8, 15687. doi:10.1038/ncomms15687

Zhang, L. J., Guo, K., Tang, H., Zhang, M. D., Fan, J. T., Cui, P., et al. (2019). The microstructure and mechanical properties of novel Al–Cr–Fe–Mn–Ni high-entropy alloys with trimodal distributions of coherent B2 precipitates. *Mater. Sci. Eng. A.* 757, 160–171. doi:10.1016/j.msea.2019.04.10

Zhang, Y., Li, J., Wang, J., Niu, S., and Kou, H. (2016). Hot deformation behavior of as-cast and homogenized $Al_{0.5}$CoCrFeNi high entropy alloys. *Metals.* 6, 124–131. doi:10.3390/met6110277

Zhang, Y., Li, J., Wang, J., Wang, W. Y., Kou, H., and Beaugnon, E. (2018). Temperature dependent deformation mechanisms of $Al_{0.3}$CoCrFeNi high-entropy alloy, starting from serrated flow behavior. *J. Alloys Compd.* 757, 39–43. doi:10.1016/j.jallcom.2018.04.305

Zhang, Y., Zuo, T. T., Tang, Z., Gao, M. C., Dahmen, K. A., Liaw, P. K., et al. (2014). Microstructures and properties of high-entropy alloys. *Prog. Mater. Sci.* 61, 1–93. doi:10.1016/j.pmatsci.2013.10.001

Zhao, C., Li, J., He, Y., Wang, J., Wang, W. Y., Kou, H., et al. (2020a). Effect of strong magnetic field on the microstructure and mechanical-magnetic properties of AlCoCrFeNi high-entropy alloy. *J. Alloys Compd.* 820, 425–489. doi:10.1016/j.jallcom.2019.153407

Zhao, Y. L., Yang, T., Li, Y. R., Fan, L., Han, B., Jiao, Z. B., et al. (2020b). Superior high-temperature properties and deformation-induced planar faults in a novel $L1_2$-strengthened high-entropy alloy. *Acta Mater.* 188, 517–527. doi:10.1016/j.actamat.2020.02.028

Zhou, S. C., Zhang, P., Xue, Y. F., Wang, F. C., Wang, L., Cao, T. Q., et al. (2018). Microstructure evolution of $Al_{0.6}$CoCrFeNi high entropy alloy powder prepared by high pressure gas atomization. *Trans. Nonferrous Metals Soc. China.* 28, 939–945. doi:10.1016/s1003-6326(18)64728-4

Zuo, T. T., Li, R. B., Ren, X. J., and Zhang, Y. (2014). Effects of Al and Si addition on the structure and properties of CoFeNi equal atomic ratio alloy. *J. Magn. Magn. Mater.* 371, 60–68. doi:10.1016/j.jmmm.2014.07.023

Conflict of Interest: The authors declare that the research was conducted in the absence of any commercial or financial relationships that could be construed as a potential conflict of interest.